LANGMUIR Article
Cite This: Langmuir 2018, 34, 4897−4907
pubs.acs.org/Langmuir

Viscosity Peak due to Shape Transition from Wormlike to Disklike Micelles: Effect of Dodecanoic Acid

Svetoslav E. Anachkov,[†,§] Gergana S. Georgieva,[†,§] Ludmila Abezgauz,[‡] Dganit Danino,[‡] and Peter A. Kralchevsky*[,†]

[†]Department of Chemical and Pharmaceutical Engineering, Faculty of Chemistry and Pharmacy, Sofia University, 1 James Bourchier Boulevard, Sofia 1164, Bulgaria

[‡]Faculty of Biotechnology and Food Engineering, Technion—Israel Institute of Technology, Haifa 3200000, Israel

Supporting Information

ABSTRACT: Here, we have investigated the synergistic growth of long wormlike micelles and their transformation into disklike micelles, which occurs in three-component solutions composed of sodium lauryl ether sulfate (SLES; anionic), cocamidopropyl betaine (CAPB; zwitterionic), and dodecanoic acid (HC12; nonionic). The solution rheology is characterized in terms of zero-shear viscosities and characteristic times for micellar breaking and reptation. Furthermore, the microstructure evolution, leading to the observed rheological behavior, is revealed by cryo-transmission electron microscopy (TEM) micrographs. In all cases, the CAPB-to-SLES ratio is fixed, whereas the fatty acid concentration is varied. At a certain HC12 concentration, the solution viscosity passes through a maximum. The cryo-TEM imaging indicates that wormlike micelles appear before the peak, grow further up to the peak, and finally transform into disklike aggregates (a very rare micellar structure) after the peak. The transformation of worms into disks leads to a drop in viscosity because the length-to-thickness aspect ratio of the disks is significantly lower than that of the worms. In this article, we elucidate the structure−rheology relations in micellar solutions that might be applied for the design of personal-care and household formulations.

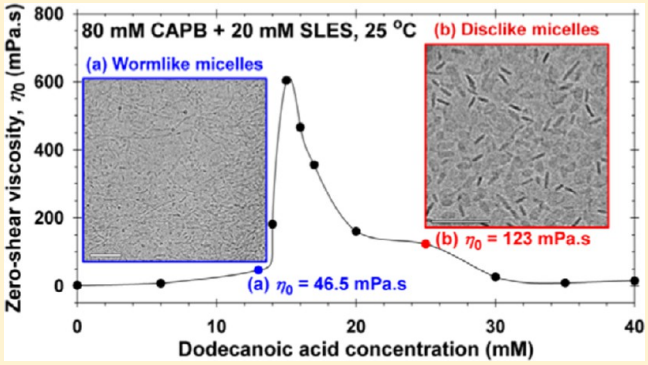

1. INTRODUCTION

Amphiphilic molecules (surfactants), when dissolved in water, self-assemble into different structures and mesophases.[1] Just above the critical micelle concentration (CMC), spherical micelles represent the dominant form of self-assembly.[1] At higher surfactant concentrations, above the so-called second CMC,[2] cylindrical, wormlike or disklike micelles appear in the solution. By increasing the surfactant concentration further, the amphiphilic molecules form liquid-crystalline mesophases, which typically appear in the following order: hexagonal, cubic, lamellar, inverted cubic, and inverted hexagonal.[1,3]

Because the liquid-crystalline phases, containing infinite aggregates, are prone to phase separation,[1] the isotropic micellar formulations are preferred in many industrial applications. For instance, isotropic worm-forming mixtures are commonly used as thickeners in cosmetics and home-care[4−6] and even as drug-delivery vehicles in biomedicine.[5] These worm-forming surfactant solutions have also attracted considerable attention because of their complex phase behavior, as well as the non-monotonic trends in their viscoelastic properties. Rehage and Hoffmann,[7,8] followed by many others,[9−34] have shown that the zero-shear viscosity of such worm-forming solutions can pass through one or even two peaks as a function of the concentration of additive.

Mechanistic understanding of the origins of the viscosity peaks was first summarized in ref 29 and then expanded in ref 35. To the left of the viscosity peak, the spherical or elongated micelles transform into cylindrical or even wormlike micelles, thus leading to a rise in viscosity. To the right of the viscosity peak, three nontrivial pathways for viscosity reduction have been found: (1) micellar branching: branches, which are not covalently bonded as in cross-linked polymers, can either form 4-fold ghostlike crossings or slide along the micelle;[25,36−39] (2) micellar shortening: the micelles decrease in size at higher additive concentrations as observed in catanionic mixtures;[4,15,29] and (3) phase or shape transition: micellar solutions transform into lyotropic mesophases or worms convert into disks.[34] The growth of rodlike micelles[40,41] and the formation of a transient network of wormlike micelles can be investigated with small-angle neutron scattering and/or dynamic light scattering.[42] To find the viscosity reduction pathway for a given surfactant mixture, direct imaging by cryo-transmission electron microscopy (TEM) could be applied.

Received: February 7, 2018
Revised: April 6, 2018
Published: April 7, 2018

DOI: 10.1021/acs.langmuir.8b00421
Langmuir 2018, 34, 4897−4907

In a previous paper,[25] we investigated the growth of giant wormlike micelles promoted by the addition of octanoic (caprylic) acid (HC8) to mixed solutions, containing sodium lauryl ether sulfate (SLES; anionic) and cocamidopropyl betaine (CAPB; zwitterionic). A high and sharp peak in the zero-shear viscosity vs the HC8 concentration plot was found. By cryogenic TEM, it was established that long threadlike micelles form before the peak and intertwined worms are present at the peak, whereas after the peak, the viscosity decreases due to the formation of multiconnected micelles.[25] Such SLES−CAPB−fatty-acid-based systems are very interesting from both fundamental and applied viewpoints[23−26,34] because they are the main components of many personal-care products and their non-monotonic rheological behavior affects the product consistency and stability. Therefore, if we understand better the physicochemical properties of such shampoolike solutions, we could devise design rules for preparing formulations with desired texture and microstructure.

In the present article, our main goal is to investigate the structure−rheology relations in three-component solutions that contain CAPB, SLES, and dodecanoic (lauric) acid (HC12) as a nonionic cosurfactant. Concerning the texture, SLES−CAPB-based systems have been recently studied in terms of their viscoelastic properties;[23−26,34,43−46] however, direct structure-specific information for the underlying microstructure is still lacking (apart from our previous paper, ref 25). For that reason, to reveal the structure−rheology (microstructure−texture) relationships, we employed here both polarized-light optical microscopy and cryogenic TEM. The latter method revealed quite different micelle morphology; instead of multiconnected micelles (as for HC8), at higher HC12 concentrations, we observed disklike micelles, which represent a very rare micellar structure.[24,34,47]

The article is structured as follows. The theory used for the interpretation of the rheological data is summarized in Section 2. The materials and experimental methods used are described in Section 3. Finally, we present and discuss the experimental results with focus on the cause-and-effect relationship between the microstructure and rheology in Section 4.

2. THEORETICAL BACKGROUND

In the semidilute regime, the rheological properties of wormlike micelles are often described by the model of Maxwell for viscoelastic bodies. According to Maxwell's model, in the regime of oscillatory shear deformations, the storage and loss moduli, G' and G'', obey the following relationships[48]

$$G' = \frac{\omega^2\tau_R^2}{1+\omega^2\tau_R^2}G_0, \quad G'' = \frac{\omega\tau_R}{1+\omega^2\tau_R^2}G_0 \tag{1}$$

where G_0 is the elastic modulus at its high-frequency plateau and ω is the angular frequency of oscillations. In this model, the magnitude of the complex viscosity, $|\eta^*|$, reads[48]

$$|\eta^*| = \frac{G_0\tau_R}{\sqrt{1+\omega^2\tau_R^2}} \tag{2}$$

An important parameter that is determined from the oscillatory deformations is the so-called crossover frequency, ω_c. At $\omega = \omega_c$, the storage and loss moduli become equal, i.e., $G' = G''$. From the last equality and eq 1, we have that $\omega_c\tau_R = 1$. Then, we find that $\tau_R = 1/\omega_c$ and $G_0 = 2G'$ at the crossover point. Knowing both G_0 and τ_R, we can determine the zero-frequency viscosity, $\eta_{\omega=0}$[7,8,48,49]

$$\eta_{\omega=0} = G_0\tau_R \tag{3}$$

The above expression for $\eta_{\omega=0}$ follows from eq 2 at $\omega = 0$. In addition, knowing G_0, the mesh size of the transient micellar network (i.e., the correlation length), ξ, can be estimated from the following expression[7,8,48,49]

$$\xi \approx \left(\frac{k_BT}{G_0}\right)^{1/3} \tag{4}$$

Furthermore, by algebraic transformations of eq 1, we see that G' and G'', which are both positive, obey the equation of a semicircle in the plane (G', G'')

$$(G' - G_{osc})^2 + G''^2 = G_{ocs}^2 \tag{5}$$

where $G_{osc} = G_0/2$. Equation 5 is thus often applied to check whether the Maxwell model is valid by plotting G'' vs G', which is also known as a Cole−Cole plot.[48,50−52]

To interpret the Cole−Cole plots, we used the Cates' model that describes the modes of stress relaxation in semidilute or concentrated micellar solutions.[49−55] In Cates' model, the stress relief processes are (i) reptation, i.e., curvilinear diffusion of a worm through the transient micellar network,[55] and (ii) reversible scission, the micelle ability to break and reform. The said processes are characterized by times for reptation τ_{rep} and for breaking τ_{break}. These characteristic times determine the ratio, $\zeta = \tau_{break}/\tau_{rep}$, as well as the overall rheological response. If $\tau_{break} \ll \tau_{rep}$, i.e., $\zeta \ll 1$, such worm-forming solutions behave as Maxwellian fluids with a single relaxation time τ_R given by[49,53]

$$\tau_R \cong (\tau_{break}\tau_{rep})^{1/2} \tag{6}$$

Deviations from the pure Maxwellian behavior of wormlike micellar solutions typically occur at high frequencies, resulting in an upturn of G''.[50−52] These deviations are typically due to the appearance of "breathing" or Rouse modes. To characterize quantitatively the departure from the ideal Maxwell model, Turner and Cates[50] defined the following parameter

$$\bar{\zeta} = \frac{\tau_{break}}{\tau_R} \tag{7}$$

By comparing experimental Cole−Cole plots with numerical calculations, one can determine $\bar{\zeta}$ and then estimate τ_{break} from viscoelastic data only using eq 7.

3. MATERIALS AND METHODS

3.1. Materials. We used cocamidopropyl betaine (CAPB; zwitterionic), M = 342.52 g/mol, with commercial name TEGO Betain F50, product of Evonik Nutrition & Care, GmbH Germany; sodium lauryl ether sulfate with one ethylene oxide group (SLES-1EO or briefly SLES; anionic), M = 332.43 g/mol, with commercial name STEOL CS-170 UB, product of Stepan Co.; and dodecanoic (lauric) acid (HC12; nonionic), M = 200.32 g/mol, product of Sigma-Aldrich, Germany. Here, CAPB and SLES are industrial-grade surfactants, whereas HC12 is of analytical grade. Figure 1 shows the structural formulas of CAPB, SLES, and HC12. As shown in ref 25, we found that 100 mM CAPB solution contains 118 ± 6 mM NaCl as an admixture (see Figure S1 in Appendix A). All chemicals were used as received without further purification. We prepared all aqueous solutions using deionized water from an Elix 3 water purification system (Merck Millipore, Merck KGaA, Germany).

DOI: 10.1021/acs.langmuir.8b00421
Langmuir 2018, 34, 4897−4907

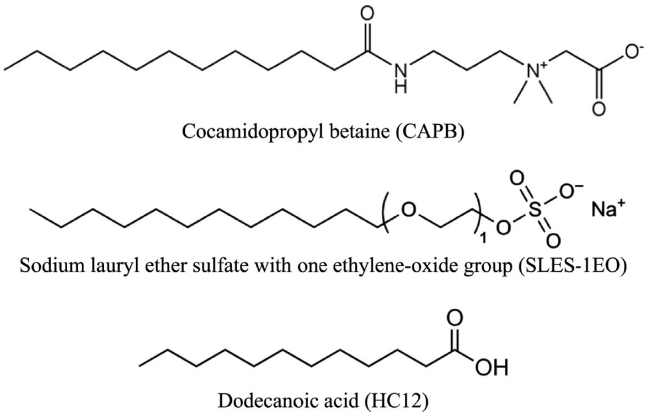

Figure 1. Structural formulas of the amphiphilic molecules used.

3.2. Solution Preparation. At a fixed CAPB/SLES molar ratio equal to 4:1, we studied the effect of fatty acid (HC12) on the micellar growth. First, we prepared the stock (binary) surfactant solution (CAPB/SLES = 4:1) in a reaction bottle, where it was homogenized by stirring at room temperature. Second, the necessary amount of dodecanoic acid (HC12) was dissolved in the mixed micelles by vigorous agitation on a temperature-controlled magnetic stirrer (at 70−75 °C) for at least 1.5 h. To reach chemical equilibrium, we kept the resulting three-component mixture in a thermostat at 25 °C for 24 h. Finally, we used the solutions for rheological and pH measurements, as well as for cryo-TEM imaging and polarized-light microscopy.

3.3. Shear Rheology. A rotational rheometer (Bohlin Gemini, Malvern Instruments, U.K.) was used to characterize the rheological properties of the micellar solutions. The experiments were carried out using a cone-and-plate geometry with plate temperature, T = 25 °C, maintained by a Peltier unit. To minimize the change in sample composition by evaporation, a solvent trap was used during each measurement. If $\eta_0 \leq 40$ Pa·s, a 60 mm cone with a cone angle of 2° (the gap distance is 70 μm) was used. If $\eta_0 > 40$ Pa·s, a 40 mm cone with a cone angle of 4° (the gap distance is 150 μm) was used instead. We then performed the rheological experiments in both (i) steady shear and (ii) oscillatory deformation regimes.

In the case of steady shear, we measured the shear stress, σ, dependence on the shear rate, $\dot{\gamma}$, in the range from 0.01 to 10 s^{-1}. Here, the apparent viscosity is defined as $\eta(\dot{\gamma}) = \sigma/\dot{\gamma}$, whereas the zero-shear viscosity, η_0, represents the limiting value of η at $\dot{\gamma} \to 0$.

In the case of oscillatory deformation (stress-controlled frequency sweep), we measured how the storage and loss moduli, G' and G'', depend on the oscillation frequency, $\nu = \omega/(2\pi)$, in the range from 0.01 to 10 Hz. For all studied samples, the viscoelastic response was linear at 2% shear-strain amplitude that was applied.

3.4. Cryo-TEM Imaging. A controlled environment vitrification system (CEVS) was used to prepare the specimens at 25 °C and 100% relative humidity. First, we placed a microliter droplet of the examined solution on a TEM grid covered with a perforated carbon film. Second, we manually blotted off the excess liquid with filter paper. The blotting duration and mode of application were tuned, so that the final film thickness did not exceed 250 nm.[56] Furthermore, to reduce the shearing effects caused by the blotting procedure, we kept the blotted samples in the CEVS for several seconds.[56] Third, we plunged the relaxed samples into liquid ethane (−183 °C) to form vitrified specimens, which we then stored in liquid nitrogen (−196 °C) until examination. All specimens were finally examined in a Tecnai T12 G^2 transmission electron microscope (FEI Co.), which operated at an acceleration voltage of 120 kV using a Gatan cryo-specimen holder that maintained the vitrified specimens below −175 °C. We used the low-dose imaging mode of the microscope to minimize the electron-beam radiation damage: the electron dose (always below 150 e/nm^2) was kept minimal, yet sufficient to record informative micrographs. DigitalMicrograph software was used to record digitally the micrographs taken on a cooled Gatan Ultrascan 1000 camera.

3.5. Light Microscopy. The phase behavior of the three-component mixtures was investigated by polarized-light optical microscopy in transmission mode. We used an optical microscope (Axioplan, Zeiss, Germany), equipped with two crossed polarizers (a polarizer and an analyzer) and a compensator (retarder), to distinguish between micellar (isotropic) and liquid-crystalline (birefringent) media. To improve visibility by introducing vivid interference colors, we placed a compensator (λ-plate or red-I plate) just below the analyzer. As a result, the micellar (isotropic) solutions appeared magenta-red without any distinct structures, whereas the liquid-crystalline (birefringent) specimens looked iridescent with textures determined by the respective mesophase.[57]

4. RESULTS AND DISCUSSION

4.1. Rheology in Steady Shear Regime. In this work, we have used a binary surfactant solution, which consists of CAPB and SLES in 4:1 molar ratio, respectively. The said CAPB-to-SLES ratio was selected because it nearly corresponds to the maximal micelle size of the binary (CAPB/SLES) system.[58] The solution's pH is ca. 5.7, and the solution viscosity is slightly above 1.7 mPa·s when the total surfactant (CAPB + SLES) concentration, c_{tot}, is 100 mM. As explained in refs 25 and 58, the viscosity of the binary (CAPB + SLES) solution is determined by the synergistic growth of rodlike micelles. Here, we will study the effect of a third component, namely, a medium-chain fatty acid (HC12), which in its nonionic form can reduce the intramicellar electrostatic repulsion and thus promote further micellar growth.[23−26,34]

In Figure 2, we examine the rheological properties of our ternary solutions in the steady shear regime. These experiments were performed at c_{tot} = 100 mM (80 mM CAPB + 20 mM SLES), whereas we varied the HC12 concentration from 0 to 40 mM. In Figure 2a, one can see the respective flow curves, where apparent viscosity η is plotted vs shear rate $\dot{\gamma}$. As seen from these flow curves, almost all solutions behave as quasi-Newtonian fluids: the viscosity stays nearly constant when the shear rate changes from 0.1 to 10 s^{-1}. Only the most viscous solution (η_0 = 603 mPa·s; with 15 mM HC12 added) is slightly shear-thinning because of the presence of wormlike micelles. These elongated micelles become aligned at high shear rates, and, as a result, the viscosity decreases. It is important to mention here that even in the most viscous solution (with 15 mM HC12) the wormlike aggregates do not seem entangled because the shear stress does not level off and the viscosity is not proportional to $\dot{\gamma}^{-1}$; for a comparison, see ref 25.

Figure 2b presents the non-monotonic trend of the zero-shear viscosity η_0 vs the HC12 concentration. As we add HC12 to the binary solution, η_0 increases and passes through a maximum at 15 mM HC12, where η_0 = 603 mPa·s (see Figure 2b). The maximal viscosity is 350 times higher than the viscosity (1.7 mPa·s) of the CAPB−SLES solution without lauric acid. Recently, viscosity peaks were also observed in CAPB−SLES mixtures with either octanoic acid[25] or lauric acid (HC12).[24]

As shown in ref 34, the viscous mixtures that contain lauric acid can form either isotropic micellar or liquid-crystalline mesophases. Here, by using polarized-light optical microscopy, we did not detect birefringence (double refraction), meaning that the studied solutions (shown in Figure 2b) are micellar (isotropic) up to 30 mM HC12. For these three-component solutions, the pH decreases from 5.7 (no HC12) to ca. 5.4 (30 mM HC12); see Figure S2a in Appendix A. Above 30 mM HC12, the solutions become opalescent because the fatty acid reaches its solubility limit in the mixed micelles and the excess

DOI: 10.1021/acs.langmuir.8b00421
Langmuir 2018, 34, 4897−4907

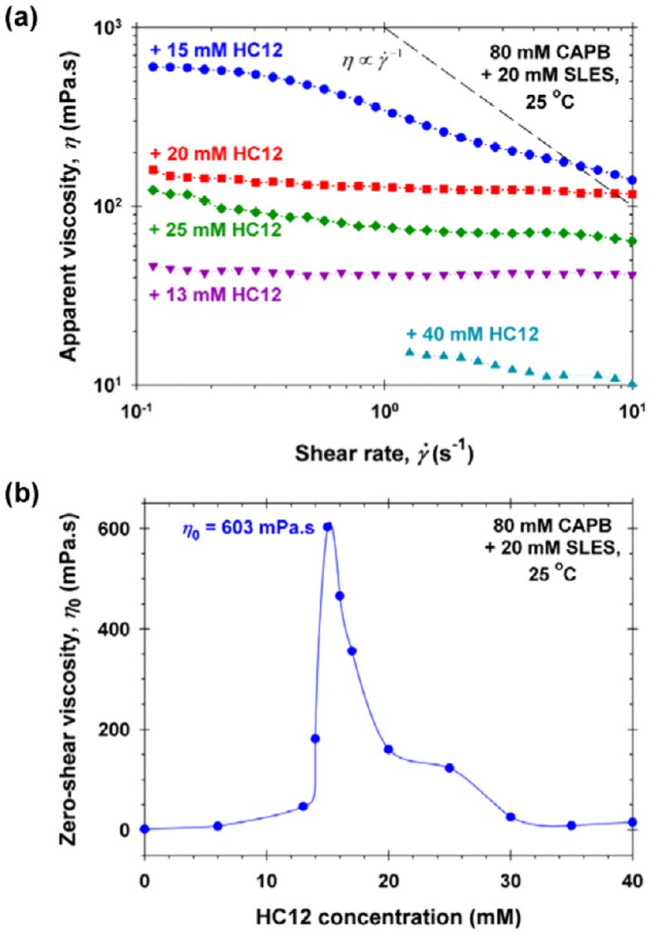

Figure 2. Effect of HC12 on the sample's shear rheology at c_{tot} = 100 mM. Plots of (a) η vs $\dot{\gamma}$ and (b) η_0 vs the HC12 concentration.

HC12 starts to form crystals in the bulk; see Figure S2 in Appendix A and ref 59. The turbid dispersions have nearly constant pH because the HC12 concentration in the bulk is fixed to 0.013 mM, which corresponds to the solubility of dodecanoic acid in water at 25 °C.[59]

Furthermore, to understand better the intricate mechanism of the micellar growth, we investigated how the ionization state of HC12 affects the solution viscosity. First, as demonstrated in Figure S2b (Appendix A), we see that the degree of HC12 ionization in the mixed micelles is less than 1.0%, meaning that the micelles accumulate the nonionic fatty acid (>99%) rather than the anionic carboxylate (<1%). Second, to directly compare the effects of HC12 and sodium laurate (NaC12) on the solution viscosity, we prepared the solutions from Figure 2 using NaC12 instead of HC12. The results, presented in Figure S3 (Appendix A), show unequivocally that NaC12 does not induce micellar growth but instead favors the formation of short rodlike or even spherical micelles. The most probable explanation is the following: NaC12 increases the intramicellar electrostatic repulsion by bringing more charges to the mixed micelles. As a result, the optimal headgroup area increases, which induces micellar shortening. Finally, the appearance of shorter rods with lower (length-to-thickness) aspect ratios leads to a drop in viscosity. In contrast, nonionic HC12 promotes micellar growth by decreasing the intramicellar electrostatic repulsion and by separating the negatively charged SLES headgroups farther apart.

Figure 3a presents our steady shear measurements for the effect of HC12 on η_0 at a fixed surfactant ratio (CAPB/SLES = 4:1) and varying total surfactant (CAPB + SLES) concentration c_{tot} from 100 to 400 mM. As one can see from the figure, the 2-fold increase of c_{tot} leads to a drastic (50 times) increase of η_0 at the peak: from 0.6 Pa·s at c_{tot} = 100 mM to 32 Pa·s at c_{tot} = 200 mM. We should note here that the peak position shifts to the

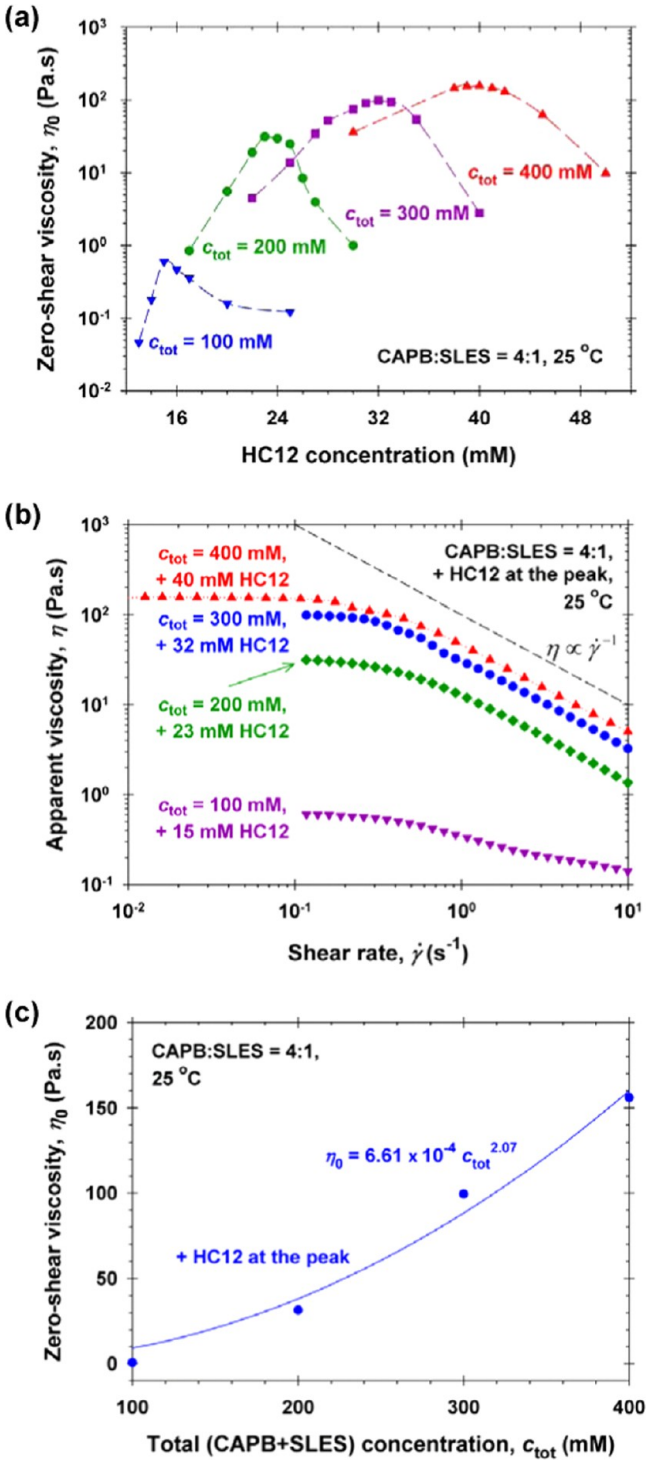

Figure 3. Effects of the HC12 concentration and c_{tot} on the viscosity at a fixed CAPB/SLES ratio equal to 4:1. Plots of (a) η_0 vs the HC12 concentration, (b) η vs $\dot{\gamma}$ at the peaks, and (c) η_0 vs c_{tot} at the peaks. In (c), the solid line depicts a power-law relationship that fits the data.

DOI: 10.1021/acs.langmuir.8b00421
Langmuir 2018, 34, 4897−4907

right as follows: 15 mM HC12 at c_{tot} = 100 mM; 23 mM HC12 at c_{tot} = 200 mM; 32 mM HC12 at c_{tot} = 300 mM; and 40 mM HC12 at c_{tot} = 400 mM. As one can notice, the peak position depends linearly on c_{tot} but with a nonzero intercept. Hereafter, the rheological behavior is examined at a fixed ratio, 4:1 CAPB/SLES, and at fatty acid concentrations corresponding to the viscosity peak at the respective c_{tot}.

In Figure 3b,c, we present how the flow curves, $\eta(\dot{\gamma})$, and the zero-shear viscosity, η_0, depend on the total (CAPB + SLES) concentration, c_{tot}, where the HC12 concentration corresponds to the peak position. From Figure 3b, one can see that the flow curves for $c_{tot} \geq 200$ mM have two distinct regions: (i) at low shear rates, $\dot{\gamma} < \dot{\gamma}_N$, $\eta \approx \eta_0$ (plateau value) and (ii) at high shear rates, $\dot{\gamma} > \dot{\gamma}_N$, $\eta \propto \dot{\gamma}^{-1}$ (the shear stress σ becomes nearly constant, known as shear-banding). Such behavior is typically associated with entangled wormlike micelles in solution.[23,25,28] In Figure S4 in Appendix A, one can find additional data for the shear stress vs shear rate, which illustrate a typical shear-banding behavior.

In Figure 3c, we continue with the effect of c_{tot} on η_0, where the HC12 concentration corresponds to the peak position. As expected, η_0 rises with c_{tot}, e.g., at c_{tot} = 100 mM, η_0 = 0.6 Pa·s, whereas at c_{tot} = 400 mM, η_0 = 160 Pa·s. The data follow a power-law relationship, $\eta_0 \propto c_{tot}^{2.1}$. The power-law index of 2.1 is closer to the values 1−2 measured for multiconnected micelles[37] than to the values 3.5−3.7 for one-component wormlike micelles.[49,52]

4.2. Rheology in Oscillatory Regime. Here, we will discuss the rheological properties of the ternary solutions obtained in the oscillatory regime. As before, the molar CAPB/SLES ratio is equal to 4:1 and the HC12 concentration corresponds to the peak position for a given total surfactant concentration c_{tot}. We should mention here that for c_{tot} = 100 mM the obtained rheological data are very noisy because of the sensitivity of our rheometer; hence, these results are deemed unreliable and are not presented below.

In Figure 4a (for c_{tot} = 200 and 400 mM) and Figure S5a (for c_{tot} = 300 mM), we see how the storage and loss moduli, G' and G'', depend on the angular frequency, ω, at 2% shear-strain amplitude, for which the viscoelastic response of the samples is still linear. As one can see from these plots, the studied three-component mixtures are viscoelastic: they are fluidlike ($G'' > G'$) at low frequencies and solidlike ($G' > G''$) at high frequencies. From each plot, we can determine the crossover frequency, ω_c, where $G' = G''$. Knowing ω_c, the relaxation time can be estimated from the following relationship: $\tau_R = 1/\omega_c$; see Section 2.

The relaxation time, τ_R, as well as the plateau modulus, G_0, can be determined in a more reliable way (using more experimental data, not just the crossing point) by simultaneously fitting $G'(\omega)$ and $G''(\omega)$ up to the crossing point with the Maxwell model described by eq 1. In such a way, τ_R and G_0 are determined as adjustable parameters from the fit and the solid lines in Figures 4a and S5a (Appendix A) are calculated. In Table 1, in the second and third columns, one can find the estimated values for G_0 and τ_R. From these results, we see that G_0 increases monotonically from 15 to 150 Pa as a function of c_{tot}, following a power-law dependence with an exponent of 2.8 ± 0.4. The latter is slightly higher but still in good agreement with the value of 2.3 ± 0.2 expected from refs 49 and 52, as well as with the value of 2.25 determined in ref 60. In contrast to G_0, τ_R decreases monotonically from 1.7 to 0.89 s with c_{tot}, also following a power-law dependence with an exponent of −0.8 ± 0.2.

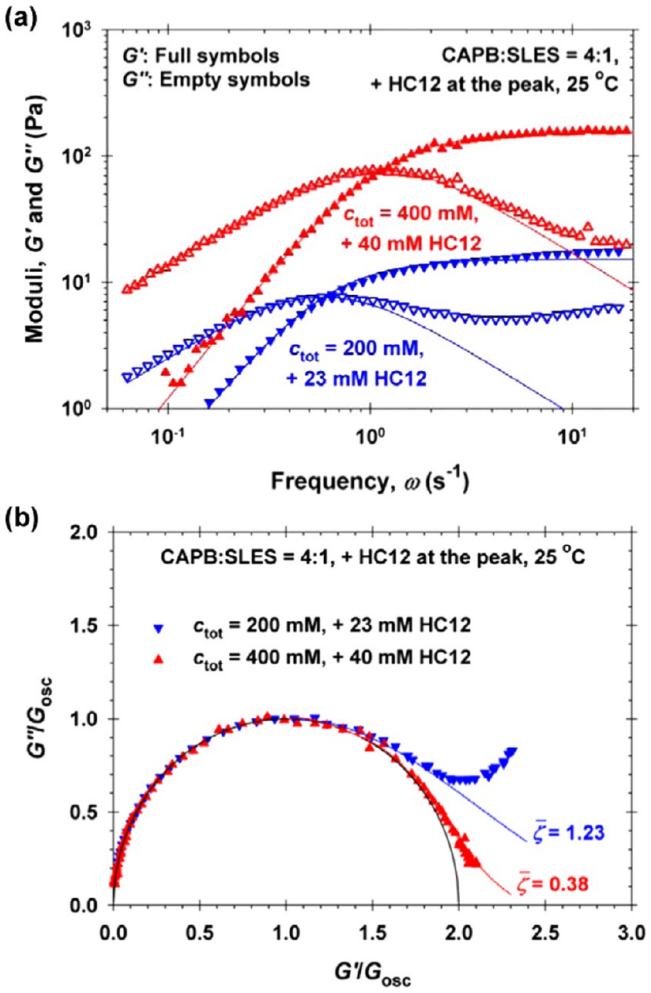

Figure 4. Effect of c_{tot} on the rheology in the oscillatory regime. Here, c_{tot} = 200 and 400 mM, whereas the HC12 concentration corresponds to the respective viscosity peak position. (a) G' and G'' are plotted vs ω; the solid lines are the best fits with the Maxwell model. (b) Cole−Cole plots of G''/G_{osc} vs G'/G_{osc}, where $G_{osc} = G_0/2$ and the solid lines are fits of numerical data from refs 50 and 52, whereas the semicircle shows pure Maxwellian behavior.

Knowing the values of G_0 (see Table 1) and using eq 4, the mesh size of the transient micellar network, ξ, can be calculated. As one can see from the fourth column in Table 1, ξ decreases nearly 2 times, from about 65 to 30 nm, as c_{tot} increases, that is, the characteristic distances between the worms diminish with the micelle volume fraction. Given G_0 and τ_R, we can substitute them in eq 3 and estimate the zero-frequency viscosity, $\eta_{\omega=0}$. For the sake of comparison, the values of $\eta_{\omega=0}$ and η_0 are presented in the fifth and sixth columns of Table 1, respectively. Here, we remind that η_0 is determined from the steady shear experiments at low $\dot{\gamma}$, whereas $\eta_{\omega=0}$ is obtained independently from the oscillatory experiments. As we notice from Table 1, $\eta_{\omega=0}$ and η_0 coincide within 20%, which is to be expected in the linear viscoelastic regime and also follows from the limiting case of the Cox−Merz rule.[48,61]

Next, we studied the mechanisms for micelle stress relaxation: breaking (or reversible scission) and reptation. These mechanisms are often characterized by parameter $\bar{\zeta}$, introduced by Turner and Cates.[50] $\bar{\zeta}$ is then related to ζ, as well

DOI: 10.1021/acs.langmuir.8b00421
Langmuir 2018, 34, 4897−4907

Table 1. Rheological Properties of the Studied Micellar Solutions, Where the Total (CAPB + SLES) Concentration, c_{tot}, Varies from 200 to 400 mM and the Dodecanoic Acid (HC12) Concentration Corresponds to the Respective Viscosity Peak Position

c_{tot} (mM)	G_0 (Pa)	τ_R (s)	ξ (nm)	$\eta_{\omega=0}$ (Pa·s)	η_0 (Pa·s)	$\bar{\zeta}$	ζ	τ_{break} (s)	τ_{rep} (s)
200	15	1.7	65	26	32	1.23	0.30	2.1	6.9
300	72	1.3	39	96	99	0.70	0.10	0.94	9.4
400	150	0.89	30	140	160	0.38	0.03	0.34	11

as to the characteristic times for micelle breaking τ_{break} and for micelle reptation τ_{rep}; see Section 2. The procedure to obtain $\bar{\zeta}$ is as follows:

(1) The experimental data from the oscillatory regime are depicted as a Cole−Cole plot (G''/G_{osc} vs G'/G_{osc}). In the case of ideal Maxwell body (see eq 5), the experimental data should collapse on a semicircle of radius $G_{osc} = G_0/2$. At high frequencies (high G'), deviations from the semicircle may occur, which are described by $\bar{\zeta}$.

(2) To find $\bar{\zeta}$, one should compare the experimental vs the theoretical Cole−Cole plots (for $\bar{\zeta}$ = 0.13, 0.38, 0.70, 1.23, 2.38, 4.61, and 10.2); see refs 50 and 52.

(3) As a result, $\bar{\zeta}$ can be estimated. Then, ζ is found from the values listed in refs 50 and 52 and the characteristic times are calculated: $\tau_{break} = \bar{\zeta}\tau_R$ (see eq 7) and $\tau_{rep} = \tau_{break}/\zeta$ ($\zeta = \tau_{break}/\tau_{rep}$; Section 2).

In Figure 4b (for c_{tot} = 200 and 400 mM) and Figure S5b (for c_{tot} = 300 mM), we have constructed the respective Cole−Cole plots, where the symbols represent our rheological measurements and the solid lines correspond to numerical calculations from refs 50 and 52. As a result of the above comparison, $\bar{\zeta}$ and ζ are now known and are given in Table 1 (in the seventh and eighth columns, respectively). Having obtained $\bar{\zeta}$ and ζ, we estimated the characteristic times for reversible scission, τ_{break}, and for reptation, τ_{rep}. We should stress here that τ_{break} was estimated solely from rheology using Cates' theory.[50] For the characteristic times, Cates' theory[49] predicts that $\tau_{break} \propto \bar{L}^{-1}$ and $\tau_{rep} \propto \bar{L}^3$, where $\bar{L}$ is the average micellar length. For rodlike and wormlike micelles, we also have that $\bar{L} \propto (c_{tot})^{1/2}$; see, e.g., refs 1 and 24. Therefore, τ_{break} should decrease with c_{tot}, whereas τ_{rep} is expected to increase with c_{tot}. Both qualitative predictions are in concurrence with the tendencies of our results (last two columns) in Table 1.

4.3. Cryo-TEM Imaging. We employed cryogenic TEM to acquire direct structure-specific information for the microstructure evolution occurring at c_{tot} = 100 mM, while we vary the HC12 concentration. At c_{tot} higher than 200 mM (~6.8 wt %), the cryo-TEM imaging becomes complicated because (i) the preparation of thin vitrified specimens is very challenging and (ii) the two-dimensional cryo-TEM micrographs become crowded due to overlapping micelles. The cryo-TEM images shown below were taken at 0 and 13 mM HC12, before the peak, as well as at 20, 25, and 40 mM HC12, after the peak; see Figure 2b. (The preparation of a vitrified sample exactly at the viscosity peak turned out to be a considerable challenge.)

Figure 5a (at 0 mM HC12) and Figure 5b (at 13 mM HC12) show typical cryo-TEM micrographs taken to the left of the peak. In Figure 5a (η_0 = 1.7 mPa·s), spherical, ca. 6 nm in diameter, and short wormlike, up to 200 nm in length, micelles coexist. This is in accord with the theoretical predictions[1,24] and with the previous experimental work of Christov et al.[58] It should be noted that almost all elongated micelles in Figure 5a appear to have a dumbbell-like shape, worms with swollen endcaps. Similar self-assembly structures with swollen endcaps have been also observed by cryo-TEM imaging in refs 29, 35, 56, 62, and 63.

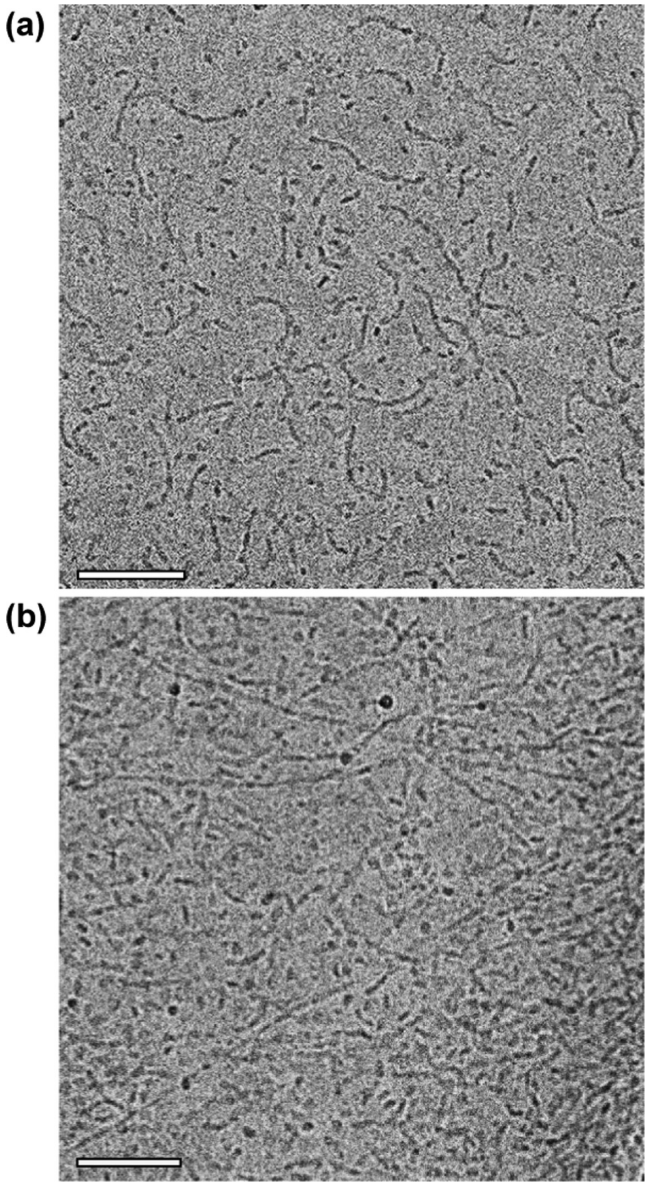

Figure 5. Cryo-TEM micrographs before the viscosity peak; 80 mM CAPB; 20 mM SLES; 100 nm scale bars. (a) No added HC12; η_0 = 1.7 mPa·s; rodlike and short wormlike micelles coexist with spherical micelles. (b) 13 mM added HC12; η_0 = 46 mPa·s; several long worms, reaching up to 0.5 μm in length, are in equilibrium with many short rods.

Figure 5b (η_0 = 46 mPa·s) shows that the micellar growth is promoted by the addition of lauric acid (HC12), which serves as a nonionic spacer between the negatively charged headgroups of SLES. In the presence of 13 mM HC12, the aggregates transform from short rods to long wormlike

DOI: 10.1021/acs.langmuir.8b00421
Langmuir 2018, 34, 4897−4907

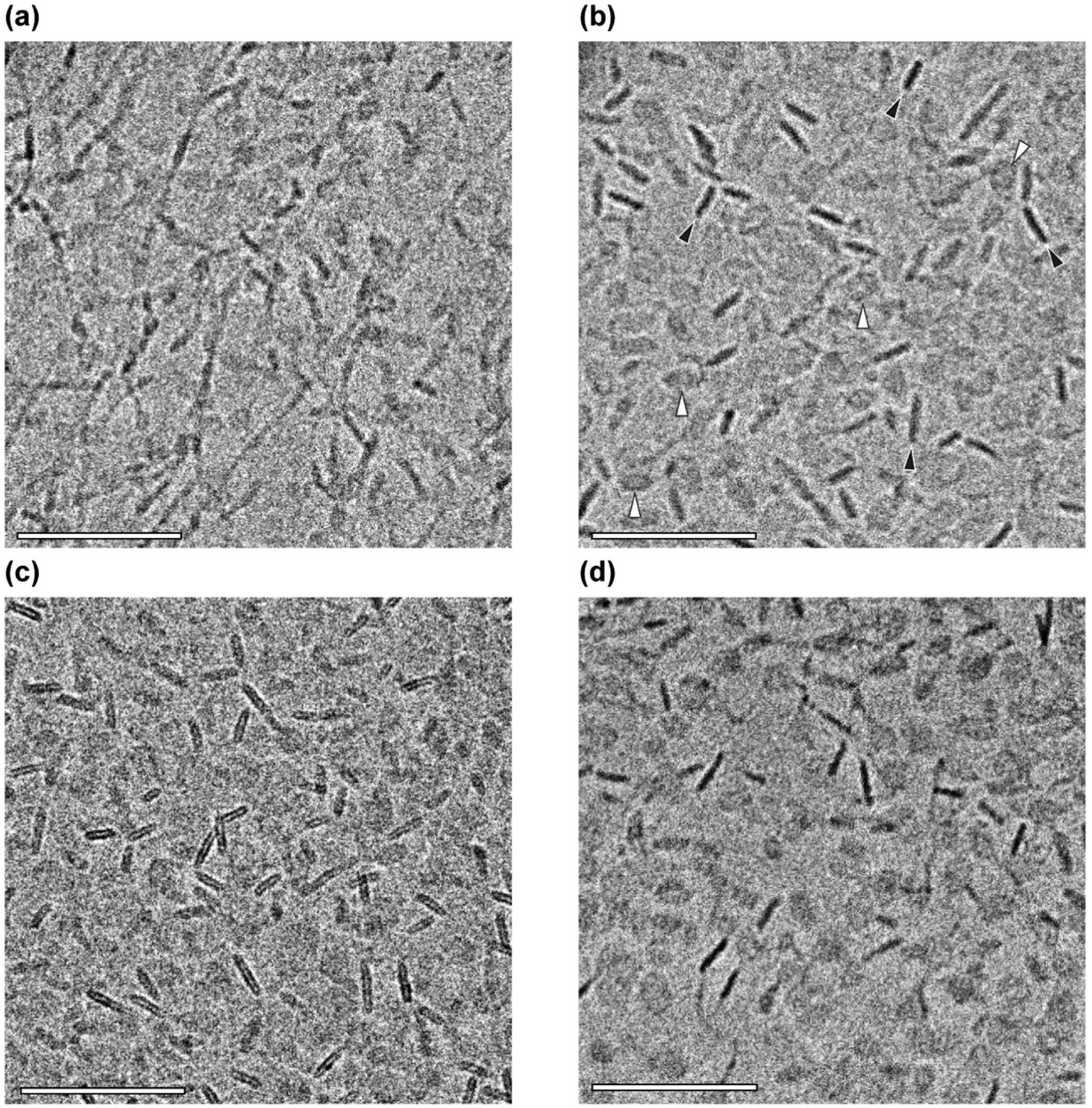

Figure 6. Cryo-TEM micrographs after the viscosity peak; 80 mM CAPB; 20 mM SLES; 100 nm scale bars. (a) 20 mM HC12 added; η_0 = 160 mPa·s; ribbonlike micelles with undulating thickness. (b, c) 25 mM HC12 added; η_0 = 120 mPa·s; disklike micelles with parallel (black arrowheads) and perpendicular (white arrowheads) orientations with respect to the electron beam. In (c), we see the boundary (thin white line) between the two surfactant layers in a given disk. (d) 40 mM HC12 added; η_0 = 15 mPa·s; disklike micelles with different orientations with respect to the electron beam.

micelles, reaching up to 0.5 μm in length; see Figure 5b. These observations prove that in the vicinity of the viscosity peak the length-to-thickness aspect ratio of the micelles increases abruptly from less than 35 to nearly 85. As a consequence, the effective volume fraction of the micelles, depending on the micelle aspect ratio and on the flow conditions, increases and so does the zero-shear viscosity, η_0.

Next, we will discuss the structures that form to the right of the peak; see Figure 6. In Figure 6a (at 20 mM HC12; η_0 = 160 mPa·s), we see flat ribbonlike structures as in ref 63. The formation of ribbons could be driven by the segregation of the different components along the micelle and/or by the addition of HC12 that imparts flatness to the micelles. Moreover, these ribbons seem to represent an intermediate state from worms to disks.

Indeed, as shown in Figure 6b,c (both at 25 mM HC12; η_0 = 120 mPa·s), the micelles transform from worms (at the peak) to disks. This transformation leads to a drop in viscosity because the diameter-to-thickness aspect ratio of the disks (<10) is much lower than the aspect ratio of the worms (>85). Figure 6b distinctively shows disks in different orientations: parallel (black arrowheads) and perpendicular (white arrowheads) with respect to the electron beam. In Figure 6c, we can

DOI: 10.1021/acs.langmuir.8b00421
Langmuir 2018, 34, 4897−4907

even distinguish the two surfactant monolayers (separated by a thin white line) that form the discoidal micelles.

Analogously, in Figure 6d (at 40 mM HC12; η_0 = 15 mPa·s), the dominant form of self-assembly is still discoidal aggregates. Because the HC12 concentration exceeds its solubility limit in the micelles, the samples are turbid and the disks coexist with fatty acid crystals.

In summary, the changes in the microstructure of the micellar solutions that contain 80 mM CAPB, 20 mM SLES, and varying concentration of fatty acid (HC12) are presented in Figure 7. To the left of the viscosity peak (see Figure 2b), we

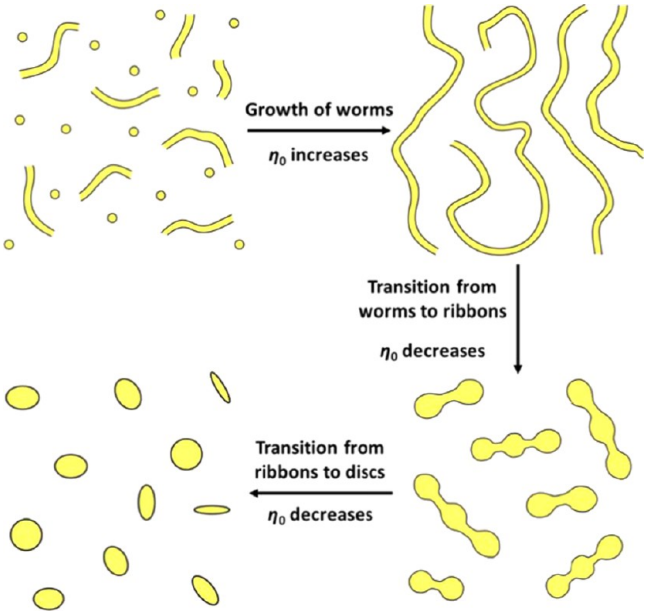

Figure 7. Schematic illustration of the microstructure evolution that occurs in the micellar solutions, containing 80 mM CAPB, 20 mM SLES, and varying concentration of HC12.

first have spherical and short wormlike micelles that transform into longer worms (Figures 5b and 7). Here, the synergistic micellar growth is induced by the addition of fatty acid. At some point, to the right of the viscosity peak, long flat ribbons are formed (Figures 6a and 7), which then break into disks (Figures 6b,c,d and 7). Such ribbonlike micelles have been directly observed via cryo-TEM.[63] Finally, at high enough concentrations of HC12, the discoidal micelles (Figures 6b,c,d and 7) become the dominant form of surfactant self-assembly.

The uniformity of the disks evidences for the existence of a minimum in the free energy of the system at a certain value of the disk radius. Qualitatively, the optimal disk radius is determined by the balance of two opposing effects. The incorporation of more surfactant molecules in the energetically favorable disk (lamellar) zone promotes micellar growth, but the growth is limited by the rising positive peripheral energy of the micelle.[24]

Here, we should stress that the microstructure evolution in the presence of a medium-chain fatty acid (such as HC12) differs from the structural changes in the presence of a short-chain fatty acid (e.g., octanoic acid or HC8); see ref 25. At high fatty acid concentrations, to the right of the respective viscosity peak, HC8 favors the formation of branched or multiconnected micelles, whereas HC12 promotes the formation of flatter ribbonlike or even disklike aggregates. Given that both fatty acids have a similar headgroup cross-sectional area, one might expect that the longer one (HC12) has a nearly cylindrical packing shape, whereas the shorter one (HC8) more closely resembles a truncated cone; see Table 20.3 in ref 1. Then, from ref 1, we know that cylindrically shaped molecules pack into bilayers or disks, whereas molecules that resemble truncated cones assemble into rodlike (or wormlike) micelles.

5. CONCLUSIONS

Here, we studied the rapid micellar growth in three-component surfactant solutions, containing zwitterionic (CAPB), anionic (SLES), and nonionic (HC12) surfactants. We investigated the effect of fatty acid (HC12) on the solution rheology and microstructure at a fixed 4:1 CAPB/SLES molar ratio. As in other surfactant-based mixtures,[7−34] the zero-shear viscosity, η_0, of our ternary mixtures follows a non-monotonic trend as a function of the fatty acid concentration. At 100 mM total (CAPB + SLES) concentration, we found a high viscosity peak: $\eta_0 \approx 603$ mPa·s at 15 mM HC12 (see Figure 2b). This viscosity is 350 times higher than the viscosity of the CAPB−SLES solution without fatty acid (HC12) and increases further with the total surfactant concentration (Figure 3).

Using polarized-light microscopy, we proved that all three-component mixtures up to 30 mM HC12 are micellar (isotropic), rather than liquid-crystalline (birefringent). In the concentration range from 30 to 40 mM HC12, the surfactant micelles coexist with fatty acid crystals because HC12 exceeds its solubility limit in the micelles. Comparing our ternary system to a similar one studied in ref 34 (see Appendix A, Figures S6 and S7), we found that the origin of our viscosity peak is not due to a transition from an isotropic micellar to a liquid-crystalline mesophase but rather due to shortening of the micelles (worms transform into disks). A similar mechanism of micelle shortening, where worms transform into spherical micelles, was directly observed in catanionic mixtures by Ziserman et al.[29]

Employing oscillatory and steady-shear rheological measurements, we demonstrated that all studied surfactant mixtures are viscoelastic and follow the Maxwell viscoelastic model in a wide range of frequencies. For total (CAPB + SLES) concentrations $c_{tot} \geq 200$ mM, the shear stress levels off (shear-banding) and $\eta \propto \dot{\gamma}^{-1}$ at high shear rates, which is typically associated with intertwined wormlike micelles.[23,25,28,64] However, Maxwellian behavior and shear-banding response have also been detected with mixtures containing disklike structures.[34] Therefore, cryogenic TEM imaging was applied to acquire structure-specific information and to relate the microstructure evolution to the non-monotonic rheological trends in viscosity.

Indeed, the cryo-TEM imaging uncovered the structural transformations causing the non-monotonic rheological trends. Before the viscosity peak, we first have spherical and short wormlike micelles that transform into longer worms. At some point, after the viscosity peak, flat ribbonlike structures form as an intermediate state from worms to disks. Finally, at high enough concentrations of fatty acid (HC12), the discoidal micelles become the dominant form of surfactant self-assembly. The formation of disks leads to a drop in viscosity because their length-to-thickness aspect ratio (or effective volume fraction) is significantly lower than that of wormlike micelles. We should also stress here that the discoidal micelles represent a very rare self-assembly structure and there are few papers[35,63,65−70] showing cryo-TEM micrographs of such aggregates.

DOI: 10.1021/acs.langmuir.8b00421
Langmuir 2018, 34, 4897−4907

To the best of our knowledge, this is the second article that studies SLES−CAPB−fatty-acid mixtures thoroughly by both cryo-TEM imaging and rheological measurements, despite the wide applications of such mixtures in many industrial products such as shampoos, body washes, etc. (The first article is also a paper of ours,[25] where SLES−CAPB−octanoic-acid mixtures were studied.) Furthermore, the current results elucidate the structure−rheology relationships in multicomponent surfactant formulations forming various microstructures. Moreover, we established that by varying the micelle composition and/or the cosurfactant charge (HC12 vs NaC12) one can alter both the intramicellar interactions and the molecular packing within the micelle, thus causing drastic changes in both solution's rheology and microstructure. Such observations could serve as guiding principles for the design of low-surfactant formulations with applications in household and personal-care detergency.

■ ASSOCIATED CONTENT

Supporting Information

The Supporting Information is available free of charge on the ACS Publications website at DOI: 10.1021/acs.langmuir.8b00421.

Additional experimental and numerical results; electrolytic conductivity measurements; NMR measurements, spectra; polarized-light microscopy images, and interpretation (PDF)

■ AUTHOR INFORMATION

Corresponding Author

*E-mail: pk@lcpe.uni-sofia.bg. Phone: (+359) 2-8161262. Fax: (+359) 2-9625643.

ORCID

Svetoslav E. Anachkov: 0000-0002-2417-1539

Peter A. Kralchevsky: 0000-0003-3942-1411

Author Contributions

§S.E.A. and G.S.G. contributed equally.

Author Contributions

P.A.K. and S.E.A. devised and defined the study. G.S.G. performed all rheological, pH, and conductivity measurements. S.E.A. interpreted the rheological, pH, and conductivity data. L.A. prepared the vitrified specimens and carried out the cryo-TEM imaging. D.D. and S.E.A. analyzed the cryo-TEM micrographs. S.E.A. and P.A.K. wrote the manuscript.

Notes

The authors declare no competing financial interest.

■ ACKNOWLEDGMENTS

We thank Dr. Ellina Kesselman and Dr. Inbal Abutbul-Ionita (both from the Technion, IIT) for their help with the cryo-TEM imaging; Mariana Paraskova (Sofia University) for the drawings in Figure 7; Prof. Pavleta Shestakova (Bulgarian Academy of Sciences) for the NMR measurements; and Prof. Krassimir Danov (Sofia University) for the very useful discussions. S.E.A. acknowledges the financial support from EU COST Action CM1101 (via an STSM travel grant) for the research visit to the Technion, IIT, Haifa, Israel. S.E.A., G.S.G., and P.A.K. gratefully acknowledge the support from the Horizon 2020 project ID: 692146-H2020-eu.4.b "Materials Networking".

■ REFERENCES

(1) Israelachvili, J. N. *Intermolecular and Surface Forces*; Academic Press: London, 2011.

(2) Lianos, P.; Zana, R. Fluorescence probe studies of the effect of concentration on the state of aggregation of surfactants in aqueous solution. *J. Colloid Interface Sci.* **1981**, *84*, 100−107.

(3) Davis, H. T.; Bodet, J. F.; Scriven, L. E.; Miller, W. G.; Microemulsions and Their Precursors. In *Physics of Amphiphilic Layers*; Meunier, J., Langevin, D., Boccara, N., Eds.; Springer Proceedings in Physics, Springer-Verlag: Berlin, 1987; Vol. *21*, p 310.

(4) Magid, L. J. The surfactant−polyelectrolyte analogy. *J. Phys. Chem. B* **1998**, *102*, 4064−4074.

(5) Dreiss, C. A. Wormlike micelles: where do we stand? Recent developments, linear rheology and scattering techniques. *Soft Matter* **2007**, *3*, 956−970.

(6) Yang, J. Viscoelastic wormlike micelles and their applications. *Curr. Opin. Colloid Interface Sci.* **2002**, *7*, 276−281.

(7) Rehage, H.; Hoffmann, H. Rheological properties of viscoelastic surfactant systems. *J. Phys. Chem.* **1988**, *92*, 4712−4719.

(8) Rehage, H.; Hoffmann, H. Viscoelastic surfactant solutions: Model systems for rheological research. *Mol. Phys.* **1991**, *74*, 933−973.

(9) Clausen, T. M.; Vinson, P. K.; Minter, J. R.; Davis, H. T.; Talmon, Y.; Miller, W. G. Viscoelastic micellar solutions: microscopy and rheology. *J. Phys. Chem.* **1992**, *96*, 474−484.

(10) Candau, S. J.; Oda, R. Linear viscoelasticity of salt-free wormlike micellar solutions. *Colloids Surf., A* **2001**, *183−185*, 5−14.

(11) Candau, S. J.; Khatory, A.; Lequeux, F.; Kern, F. Rheological behaviour of wormlike micelles: effect of salt content. *J. Phys. IV France* **1993**, *03*, 197−209.

(12) Ali, A. A.; Makhloufi, R. Linear and nonlinear rheology of an aqueous concentrated system of cethyltrimethylammonium chloride and sodium salicylate. *Phys. Rev. E* **1997**, *56*, 4474−4478.

(13) Hartmann, V.; Cressely, R. Linear and non-linear rheology of a wormlike micellar system in presence of sodium tosylate. *Rheol. Acta* **1998**, *37*, 115−121.

(14) Aswal, V. K.; Goyal, P. S.; Thiyagarajan, P. Small-angle neutron-scattering and viscosity studies of CTAB/NaSal viscoelastic micellar solutions. *J. Phys. Chem. B* **1998**, *102*, 2469−2473.

(15) Cappelaere, E.; Cressely, R. Influence of $NaClO_3$ on the rheological behaviour of a micellar solution of CPCl. *Rheol. Acta* **2000**, *39*, 346−353.

(16) Croce, V.; Cosgrove, T.; Maitland, G.; Hughes, T.; Karlsson, G. Rheology, cryogenic transmission electron spectroscopy, and small-angle neutron scattering of highly viscoelastic wormlike micellar solutions. *Langmuir* **2003**, *19*, 8536−8541.

(17) Angelescu, D.; Khan, A.; Caldararu, H. Viscoelastic properties of sodium dodecyl sulfate with aluminum salt in aqueous solution. *Langmuir* **2003**, *19*, 9155−9161.

(18) Hoffmann, H.; Rauscher, A.; Gradzielski, M.; Schulz, S. F. Influence of ionic surfactants on the viscoelastic properties of zwitterionic surfactant solutions. *Langmuir* **1992**, *8*, 2140−2146.

(19) Acharya, D. P.; Hattori, K.; Sakai, T.; Kunieda, H. Phase and rheological behavior of salt-free alkyltrimethylammonium bromide/alkanoyl-N-methylethanolamide/water systems. *Langmuir* **2003**, *19*, 9173−9178.

(20) Afifi, H.; Karlsson, G.; Heenan, R. K.; Dreiss, C. A. Solubilization of oils or addition of monoglycerides drives the formation of wormlike micelles with an elliptical cross-section in cholesterol-based surfactants: A study by rheology, SANS, and cryo-TEM. *Langmuir* **2011**, *27*, 7480−7492.

(21) Parker, A.; Fieber, W. Viscoelasticity of anionic wormlike micelles: effects of ionic strength and small hydrophobic molecules. *Soft Matter* **2013**, *9*, 1203−1213.

(22) Kamada, M.; Shimizu, S.; Aramaki, K. Manipulation of the viscosity behavior of wormlike micellar gels by changing the molecular structure of added perfumes. *Colloids Surf., A* **2014**, *458*, 110−116.

(23) Mitrinova, Z.; Tcholakova, S.; Popova, J.; Denkov, N.; Dasgupta, B.; Ananthapadmanabhan, K. P. Efficient control of the rheological

and surface properties of surfactant solutions containing C8−C18 fatty acids as cosurfactants. *Langmuir* **2013**, *29*, 8255−8265.
(24) Anachkov, S. E.; Kralchevsky, P. A.; Danov, K. D.; Georgieva, G. S.; Ananth-apadmanabhan, K. P. Disclike vs. cylindrical micelles: generalized model of micelle growth and data interpretation. *J. Colloid Interface Sci.* **2014**, *416*, 258−273.
(25) Georgieva, G. S.; Anachkov, S. E.; Lieberwirth, I.; Koynov, K.; Kralchevsky, P. A. Synergistic growth of giant wormlike micelles in ternary mixed surfactant solutions: Effect of octanoic acid. *Langmuir* **2016**, *32*, 12885−12893.
(26) Mitrinova, Z.; Tcholakova, S.; Denkov, N. Control of surfactant solution rheology using medium-chain cosurfactants. *Colloids Surf., A* **2018**, *537*, 173−184.
(27) Koehler, R. D.; Raghavan, S. R.; Kaler, E. W. Microstructure and dynamics of wormlike micellar solutions formed by mixing cationic and anionic surfactants. *J. Phys. Chem. B* **2000**, *104*, 11035−11044.
(28) Raghavan, S. R.; Fritz, G.; Kaler, E. W. Wormlike micelles formed by synergistic self-assembly in mixtures of anionic and cationic surfactants. *Langmuir* **2002**, *18*, 3797−3803.
(29) Ziserman, L.; Abezgauz, L.; Ramon, O.; Raghavan, S. R.; Danino, D. Origins of the viscosity peak in wormlike micellar solutions. 1. Mixed catanionic surfactants. A cryo-transmission electron microscopy study. *Langmuir* **2009**, *25*, 10483−10489.
(30) Kern, F.; Lequeux, F.; Zana, R.; Candau, S. J. Dynamic properties of salt-free viscoelastic micellar solutions. *Langmuir* **1994**, *10*, 1714−1723.
(31) Acharya, D. P.; Kunieda, H.; Siba, Y.; Aratani, K.-I. Phase and rheological behavior of novel gemini-type surfactant systems. *J. Phys. Chem. B* **2004**, *108*, 1790−1797.
(32) Acharya, D. P.; Hossain, M. K.; Feng, J.; Sakai, T.; Kunieda, H. Phase and rheological behavior of viscoelastic wormlike micellar solutions formed in mixed nonionic surfactant systems. *Phys. Chem. Chem. Phys.* **2004**, *6*, 1627−1631.
(33) Naito, N.; Acharya, D. P.; Tanimura, J.; Kunieda, H. Rheological behavior of wormlike micellar solutions in mixed nonionic systems of polyoxyethylene phytosterol-polyoxyethylene dodecyl ether. *J. Oleo Sci.* **2004**, *53*, 599−606.
(34) Colafemmina, G.; Recchia, R.; Ferrante, A. S.; Amin, S.; Palazzo, G. Lauric acid-induced formation of a lyotropic nematic phase of disk-shaped micelles. *J. Phys. Chem. B* **2010**, *114*, 7250−7260.
(35) Danino, D. Cryo-TEM of soft molecular assemblies. *Curr. Opin. Colloid Interface Sci.* **2012**, *17*, 316−329.
(36) Lequeux, F. Reptation of connected wormlike micelles. *Europhys. Lett.* **1992**, *19*, 675−681.
(37) Khatory, A.; Kern, F.; Lequeux, F.; Appell, J.; Porte, G.; Morie, N.; Ott, A.; Urbach, W. Entangled versus multiconnected network of wormlike micelles. *Langmuir* **1993**, *9*, 933−939.
(38) Appell, J.; Porte, G.; Khatory, A.; Kern, F.; Candau, S. Static and dynamic properties of a network of wormlike surfactant micelles (cetylpyridinium chlorate in sodium chlorate brine). *J. Phys. II France* **1992**, *2*, 1045−1052.
(39) Drye, T. J.; Cates, M. E. Living networks: The role of cross-links in entangled surfactant solutions. *J. Chem. Phys.* **1992**, *96*, 1367−1375.
(40) Alargova, R.; Petkov, J.; Petsev, D.; Ivanov, I. B.; Broze, G.; Mehreteab, A. Light scattering study of sodium dodecyl polyoxyethylene-2 sulfate micelles in the presence of multivalent counterions. *Langmuir* **1995**, *11*, 1530−1536.
(41) Alargova, R. G.; Petkov, J. T.; Petsev, D. N. Micellization and interfacial properties of alkyloxyethylene sulfate surfactants in the presence of multivalent counterions. *J. Colloid Interface Sci.* **2003**, *261*, 1−11.
(42) Moitzi, C.; Freiberger, N.; Glatter, O. Viscoelastic wormlike micellar solutions made from nonionic surfactants: Structural investigations by SANS and DLS. *J. Phys. Chem. B* **2005**, *109*, 16161−16168.
(43) Abdel-Rahem, R. A.; Reger, M.; Hloucha, M.; Hoffmann, H. Rheology of aqueous solutions containing SLES, CAPB, and microemulsion: Influence of cosurfactant and salt. *J. Dispersion Sci. Technol.* **2014**, *35*, 64−75.
(44) Zou, W.; Tang, X.; Weaver, M.; Koenig, P.; Larson, R. G. Determination of characteristic lengths and times for wormlike micelle solutions from rheology using a mesoscopic simulation method. *J. Rheol.* **2015**, *59*, 903−934.
(45) Tang, X.; Zou, W.; Koenig, P. H.; McConaughy, S. D.; Weaver, M. R.; Eike, D. M.; Schmidt, M. J.; Larson, R. G. Multiscale modeling of the effects of salt and perfume raw materials on the rheological properties of commercial threadlike micellar solutions. *J. Phys. Chem. B* **2017**, *121*, 2468−2485.
(46) Jiang, H.; Beaucage, G.; Vogtt, K.; Weaver, M. The effect of solvent polarity on wormlike micelles using dipropylene glycol (DPG) as a cosolvent in an anionic /zwitterionic mixed surfactant system. *J. Colloid Interface Sci.* **2018**, *509*, 25−31.
(47) Zemb, T.; Dubios, M.; Deme, B.; Guli-Kryzywicki, T. Self-assembly of flat nanodiscs in salt-free catanionic surfactant solutions. *Science* **1999**, *283*, 816−819.
(48) Larson, R. G. *The Structure and Rheology of Complex Fluids*; Oxford University Press: Oxford, 1999.
(49) Cates, M. E.; Candau, S. J. Statics and dynamics of worm-like surfactant micelles. *J. Phys.: Condens. Matter* **1990**, *2*, 6869−6892.
(50) Turner, M. S.; Cates, M. E. Linear viscoelasticity of living polymers: A quantitative probe of chemical relaxation times. *Langmuir* **1991**, *7*, 1590−1594.
(51) Granek, R.; Cates, M. E. Stress relaxation in living polymers: Results from a Poisson renewal model. *J. Chem. Phys.* **1992**, *96*, 4758−4767.
(52) Kern, F.; Lemarechal, P.; Candau, S. J.; Cates, M. E. Rheological properties of semidilute and concentrated solutions of cetyltrimethylammonium bromide in the presence of potassium bromide. *Langmuir* **1992**, *8*, 437−440.
(53) Cates, M. E. Reptation of living polymers: Dynamics of entangled polymers in the presence of reversible chain-scission reactions. *Macromolecules* **1987**, *20*, 2289−2296.
(54) Cates, M. E. Nonlinear viscoelasticity of wormlike micelles (and other reversibly breakable polymers). *J. Phys. Chem.* **1990**, *94*, 371−375.
(55) Cates, M. E.; Fielding, S. M. Rheology of giant micelles. *Adv. Phys.* **2006**, *55*, 799−879.
(56) Danino, D.; Bernheim-Groswasser, A.; Talmon, Y. Digital cryogenic transmission electron microscopy: an advanced tool for direct imaging of complex fluids. *Colloids Surf., A* **2001**, *183−185*, 113−122.
(57) Murphy, D. B.; Davidson, M. W. *Fundamentals of Light Microscopy and Electronic Imaging*; Wiley-Blackwell: New Jersey, 2012.
(58) Christov, N. C.; Denkov, N. D.; Kralchevsky, P. A.; Ananthapadmanabhan, K. P.; Lips, A. Synergistic sphere-to-rod micelle transition in mixed solutions of sodium dodecyl sulfate and cocoamidopropyl betaine. *Langmuir* **2004**, *20*, 565−571.
(59) Tzocheva, S. S.; Kralchevsky, P. A.; Danov, K. D.; Georgieva, G. S.; Post, A. J.; Ananthapadmanabhan, K. P. Solubility limits and phase diagrams for fatty acids in anionic (SLES) and zwitterionic (CAPB) micellar surfactant solutions. *J. Colloid Interface Sci.* **2012**, *369*, 274−286.
(60) Oda, R.; Narayanan, J.; Hassan, P. A.; Manohar, C.; Salkar, R. A.; Kern, F.; Candau, S. J. Effect of the lipophilicity of the counterion on the viscoelasticity of micellar solutions of cationic surfactants. *Langmuir* **1998**, *14*, 4364−4372.
(61) Cox, W. P.; Merz, E. H. Correlation of dynamic and steady flow viscosities. *J. Polym. Sci.* **1958**, *28*, 619−622.
(62) Dan, N.; Shimoni, K.; Pata, V.; Danino, D. Effect of Mixing on the Morphology of Cylindrical Micelles. *Langmuir* **2006**, *22*, 9860−9865.
(63) Danino, D.; Abezgauz, L.; Portnaya, I.; Dan, N. From Discs to Ribbons Networks: The Second Critical Micelle Concentration in Nonionic Sterol Solutions. *J. Phys. Chem. Lett.* **2016**, *7*, 1434−1439.
(64) Spenley, N. A.; Cates, M. E.; McLeish, T. C. B. Nonlinear rheology of wormlike micelles. *Phys. Rev. Lett.* **1993**, *71*, 939−942.
(65) Mazer, N. A.; Benedek, G. B.; Carey, M. C. Quasielastic light-scattering studies of aqueous biliary lipid systems. Mixed micelle

DOI: 10.1021/acs.langmuir.8b00421
Langmuir 2018, 34, 4897−4907

formation in bile salt-lecithin solutions. *Biochemistry* **1980**, *19*, 601−615.
(66) Vinson, P.; Bellare, J.; Davis, H.; Miller, W.; Scriven, L. Direct imaging of surfactant micelles, vesicles, discs, and ripple phase structures by cryo-transmission electron microscopy. *J. Colloid Interface Sci.* **1991**, *142*, 74−91.
(67) Lasic, D. D. Mixed Micelles in Drug Delivery. *Nature* **1992**, *355*, 279−280.
(68) Silvander, M.; Karlsson, G.; Edwards, K. Vesicle solubilization by alkyl sulfate surfactants: A cryo-TEM study of the vesicle to micelle transition. *J. Colloid Interface Sci.* **1996**, *179*, 104−113.
(69) Voets, I. K.; de Keizer, A.; de Waard, P.; Frederik, P. M.; Bomans, P. H. H.; Schmalz, H.; Walther, A.; King, S. M.; Leermakers, F. A. M.; Cohen Stuart, M. A. Double-faced micelles from water-soluble polymers. *Angew. Chem., Int. Ed.* **2006**, *45*, 6673−6676.
(70) Holder, S. J.; Sommerdijk, N. A. J. M. New micellar morphologies from amphiphilic block copolymers: Disks, toroids and bicontinuous micelles. *Polym. Chem.* **2011**, *2*, 1018.

DOI: 10.1021/acs.langmuir.8b00421
Langmuir 2018, 34, 4897−4907

Supporting Information

for the article

Viscosity Peak Due to Shape Transition from Wormlike to Disklike Micelles: Effect of Dodecanoic Acid

Svetoslav E. Anachkov,[§,†] Gergana S. Georgieva,[§,†] Ludmila Abezgauz,[‡] Dganit Danino,[‡], Peter A. Kralchevsky*[,†]

[†] *Department of Chemical and Pharmaceutical Engineering, Faculty of Chemistry and Pharmacy, Sofia University, 1 James Bourchier Blvd., 1164 Sofia, Bulgaria*

[‡] *Faculty of Biotechnology and Food Engineering, Technion – Israel Institute of Technology, Haifa 3200000, Israel*

[§] *Both authors contributed equally.*

* *E-mail address*: pk@lcpe.uni-sofia.bg (P.A. Kralchevsky)

Appendix A. Additional experimental and numerical results

A.1. Electrolytic conductivity measurements of TEGO® Betain F50 salt content

From the product specification data of TEGO® Betain F50 (Goldschmidt GmbH – now part of Evonik Industries AG), one can see its chemical composition: CAPB (37 – 42 wt%), NaCl (5.8 – 7.3 wt%) and water.[1] In other words, 100 mM CAPB solution contains from 81 to 120 mM NaCl. To determine the exact amount of NaCl in our batch of TEGO® Betain F50, we carried out electrolytic conductivity measurements using a conductivity meter EC 215 (Hanna Instruments – USA).[2]

Figure S1 shows that the electrolytic conductivity κ increases as a function of the CAPB concentration c_{CAPB}. At its natural $\mathrm{pH} = 5.0 \pm 0.5$,[1] CAPB is in zwitterionic (uncharged) form, meaning that the observed increase of κ is solely due to the presence of NaCl, given by:

$$c_{\mathrm{NaCl}} = x c_{\mathrm{CAPB}}\,, \tag{A.1}$$

where c_{NaCl} is the molar concentration of NaCl and x is the molar fraction of salt with respect to CAPB. Then, the conductivity κ of the studied solutions can be evaluated as follows:[3,4]

$$\kappa = \kappa_0 + \Lambda^{(0)}_{\mathrm{NaCl}} f(I) c_{\mathrm{NaCl}}\,. \tag{A.2}$$

Here, κ_0 is the background conductivity, which accounts for trace amounts of other ionic species (like H^+, OH^-, HCO_3^-) in the water used; $\Lambda^{(0)}_{\mathrm{NaCl}} = 126.39\,\mathrm{cm^2 \cdot S \cdot mol^{-1}}$ is the molar conductivity of NaCl solution at infinite dilution;[5] $f(I)$ is a correction coefficient for ion-ion

interactions; and $I = c_{NaCl}$, expressed as mol/L ≡ M, is the ionic strength. The correction factor $f(I)$ reads:[4]

$$f(I) = 1 - 0.7\sqrt{I} + 0.74I \,. \tag{A.3}$$

Using eq A.2, we fitted the experimental data shown in Figure S1. From the fit, κ_0 and x were determined as adjustable parameters, and are as follows: $\kappa_0 = 6.5 \pm 1.3$ μS·cm^{-1}, close to that of water equilibrated with CO_2, and $x = 1.18 \pm 0.06$. In the latter value, we have taken into account that the typical error of the conductivity measurement is up to 5 %.

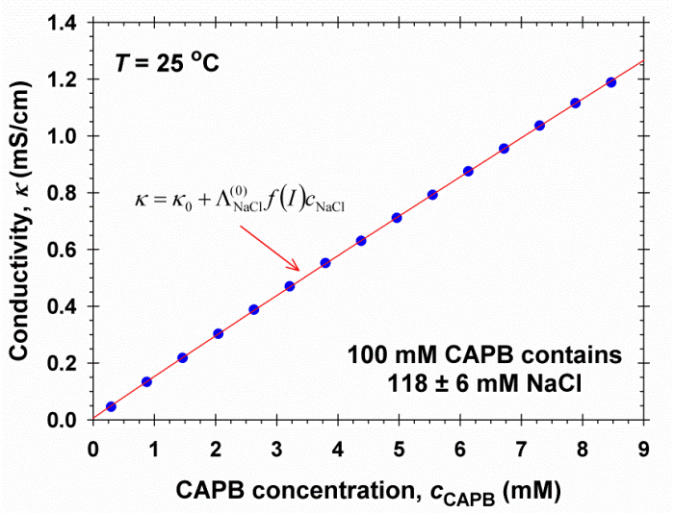

Figure S1. Plot of the electrolytic conductivity κ versus the CAPB concentration c_{CAPB}. The full circles represent the experimental data, whereas the solid line is the fit to the data using eq A.2.

A.2. Ionization states of CAPB and HC12

First, we will discuss the ionization state of CAPB since it is a pH-sensitive molecule.[2] As mentioned above, at pH = 5.0, CAPB is predominantly in zwitterionic (uncharged) form. There is only a trace amount of cationic-CAPB (c-CAPB), which can be calculated in the following way:

$$K_{a,c-CAPB} = \frac{a_{H^+} a_{CAPB}}{a_{c-CAPB}} \approx \frac{a_{H^+} c_{CAPB}}{c_{c-CAPB}} \Rightarrow \frac{c_{c-CAPB}}{c_{CAPB}} = \frac{10^{-pH}}{K_{a,c-CAPB}} \,. \tag{A.4}$$

Here, a_{H^+}, a_{CAPB}, and $a_{c\text{-}CAPB}$ are the activities of the respective species; and $K_{a,c\text{-}CAPB}$ is the acidity constant of c-CAPB. In eq A.4, we have assumed that the activity coefficients γ_{CAPB} and $\gamma_{c\text{-}CAPB}$ are equal. For a similar 1-12 carboxylate betaine, $K_{a,c\text{-}CAPB} \approx 10^{-2}$ M at 25 °C.[6] Therefore, using eq A.4, we estimate that c-CAPB should be around 0.1 % at pH = 5 and even less at higher pH.

Second, we will estimate the degree of HC12 ionization in the mixed micelles α, which consist of CAPB, SLES, and HC12. Following the approach from Refs. 2 and 7, we have that:

$$\gamma_i y_i = \frac{c_i}{K_{i,\mathrm{mic}}}, \qquad (i = \mathrm{HC12 \text{ or } C12^-}). \tag{A.5}$$

Here, γ_i and y_i are the activity coefficient and the molar fraction of component i in the micelles, respectively; c_i is the respective monomer concentration in the bulk; and $K_{i,\mathrm{mic}}$ is the micellization constant, which is related to the work for transferring of a monomer of component i from the solution into a micelle. Assuming that $\gamma_{\mathrm{HC12}} \approx \gamma_{\mathrm{C12^-}}$, from eq A.5, we obtain the relationship:

$$\frac{y_{\mathrm{C12^-}}}{y_{\mathrm{HC12}}} = \frac{c_{\mathrm{C12^-}}}{c_{\mathrm{HC12}}} \frac{K_{\mathrm{HC12,mic}}}{K_{\mathrm{C12^-,mic}}}, \tag{A.6}$$

where $K_{\mathrm{HC12,mic}} \approx 4.0 \times 10^{-5}$ M and $K_{\mathrm{C12^-,mic}} \approx 0.023$ M at 25 °C.[7] These values demonstrate that the transfer of the nonionic fatty acid (HC12) from the bulk into a micelle is much more favorable (about 600 times) than the transfer of the negatively-charged carboxylate ($\mathrm{C12^-}$). Additionally, from the condition for dissociation equilibrium between HC12 and $\mathrm{C12^-}$ in the bulk, we find that:

$$\frac{c_{\mathrm{C12^-}}}{c_{\mathrm{HC12}}} = \frac{K_{\mathrm{a,HC12}}}{10^{-\mathrm{pH}}}, \tag{A.7}$$

where $K_{\mathrm{a,HC12}} = 1.3 \times 10^{-5}$ M ($\mathrm{p}K_{\mathrm{a,HC12}} = 4.90$) is the acidity constant of HC12 at 25 °C.[8] (In fact, $\mathrm{p}K_{\mathrm{a,HC}n} = 4.90$ for $n \geq 10$.) Combining eq A.6 and A.7, the ratio $y_{\mathrm{C12^-}} / y_{\mathrm{HC12}}$ yields:

$$\frac{y_{\mathrm{C12^-}}}{y_{\mathrm{HC12}}} = \frac{K_{\mathrm{a,HC12}}}{10^{-\mathrm{pH}}} \frac{K_{\mathrm{HC12,mic}}}{K_{\mathrm{C12^-,mic}}}. \tag{A.8}$$

Finally, the degree of HC12 ionization in the mixed micelles α is given by:

$$\alpha \equiv \frac{y_{\mathrm{C12^-}}}{y_{\mathrm{C12^-}} + y_{\mathrm{HC12}}} = \frac{10^{\mathrm{pH-7.64}}}{1 + 10^{\mathrm{pH-7.64}}}. \tag{A.9}$$

Figure S2a shows how the pH of the micellar solution depends on the *input* HC12 concentration at fixed 80 mM CAPB and 20 mM SLES. Below 30 mM HC12, the micellar solutions are clear and their pH decreases logarithmically with the increase of the HC12 concentration. At 30 mM HC12, the mixed micelles are fully-loaded with dodecanoic acid; hence, any excess amount of HC12 precipitates in the form of small crystals and the sample becomes turbid. Above 30 mM HC12, the pH levels off, because the monomer concentration

c_{HC12} in the bulk is fixed to 0.013 mM, that is, the solubility of dodecanoic acid in water at 25 °C.[7,8]

Using the experimental data from Figure S2a and applying eq A.9, we calculated the degree of HC12 ionization α in the micelles as a function of the input HC12 concentration (see Figure S2b). In Figure S2b, α decreases from about 1 % to 0.6 % and then reaches a plateau. From these numerical results, we also see that the tri-component mixed micelles contain much more nonionic HC12 than negatively-charged $C12^-$, having $y_{HC12} / y_{C12^-} > 100$, while $C12^-$ is more abundant in the bulk, having $c_{HC12} / c_{C12^-} < 0.3$. As explained before, such partitioning in the micelles is to be expected since the nonionic HC12 goes more readily in the micelles than the negatively-charged carboxylate ($C12^-$).

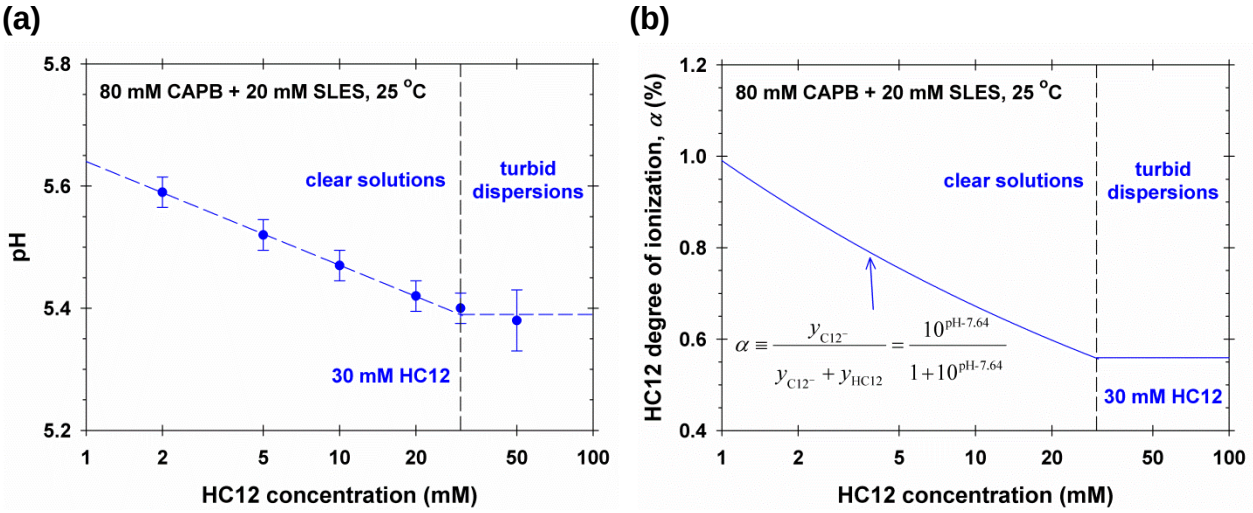

Figure S2. (a) The pH of the ternary mixtures is plotted versus the *input* HC12 concentration at fixed 80 mM CAPB and 20 mM SLES. The full circles represent the experimental data, whereas the dashed line follows the observed tendency. (b) Plot of α versus the *input* HC12 concentration at fixed 80 mM CAPB and 20 mM SLES. The solid line is calculated using eq A.9.

A.3. Effect of sodium dodecanoate (NaC12) on the micellar growth

To prove that HC12 (rather than NaC12) induces the micellar growth, we carried out additional experiments with NaC12. The samples were prepared following the experimental procedure from Section 3.2 of the paper. Figure S3 shows the results of our pH and viscosity measurements of the respective NaC12-containing systems. We see that the pH increases logarithmically, whereas η_0 decreases monotonically with the NaC12 concentration. The latter can be explained as follows: NaC12 increases the surface charge density of the mixed micelles; hence, they diminish in size due to increased intramicellar electrostatic repulsion between the negatively-charged headgroups and η_0 decreases (Figure S3).

In contrast, the nonionic HC12 decreases the surface charge density of the mixed micelles and serves as a spacer between the negatively-charged SLES headgroups, both of which lead to micellar growth; see the main text of the article.

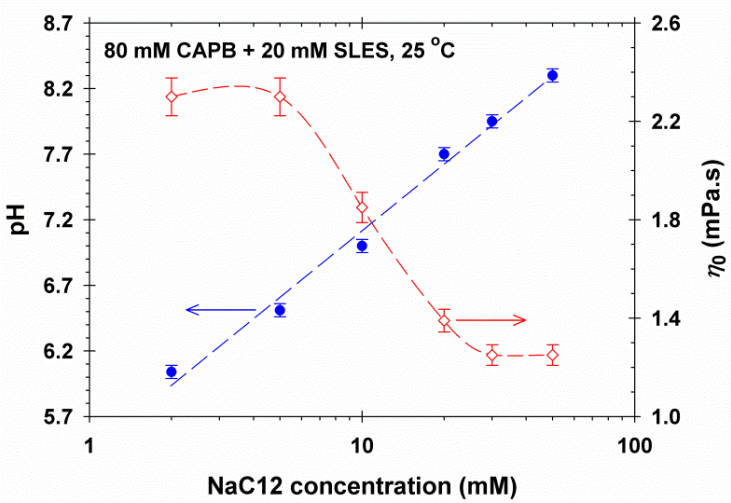

Figure S3. The pH (left *y*-axis) and the zero-shear viscosity η_0 (right *y*-axis) are plotted as a function of the *input* NaC12 concentration at fixed 80 mM CAPB and 20 mM SLES. The full circles represent the pH data, whereas the empty diamonds represent the measured viscosity η_0. The dashed lines follow the observed tendencies.

A.4. Additional rheological results

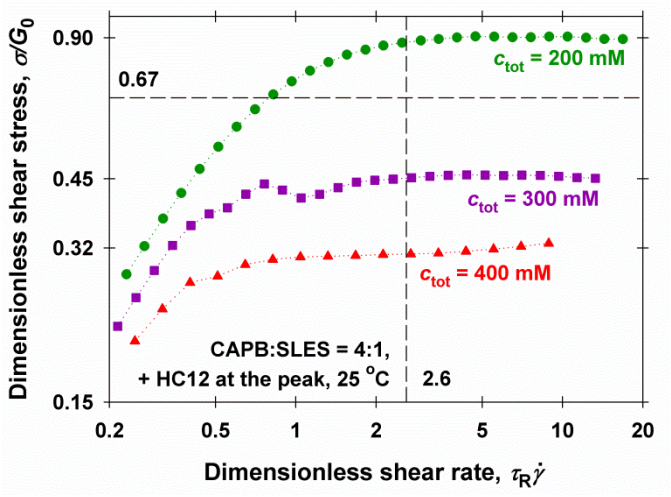

Figure S4. Rheological data for the ternary micellar solutions, for which the HC12 concentration corresponds to the viscosity peak position at the respective total surfactant (CAPB + SLES) concentration c_{tot}. The dimensionless shear stress σ / G_0 is plotted versus the dimensionless shear rate $\tau_R\dot{\gamma}$. G_0 and τ_R are determined from the oscillatory experiments; see Section 4.2 in the paper for details.

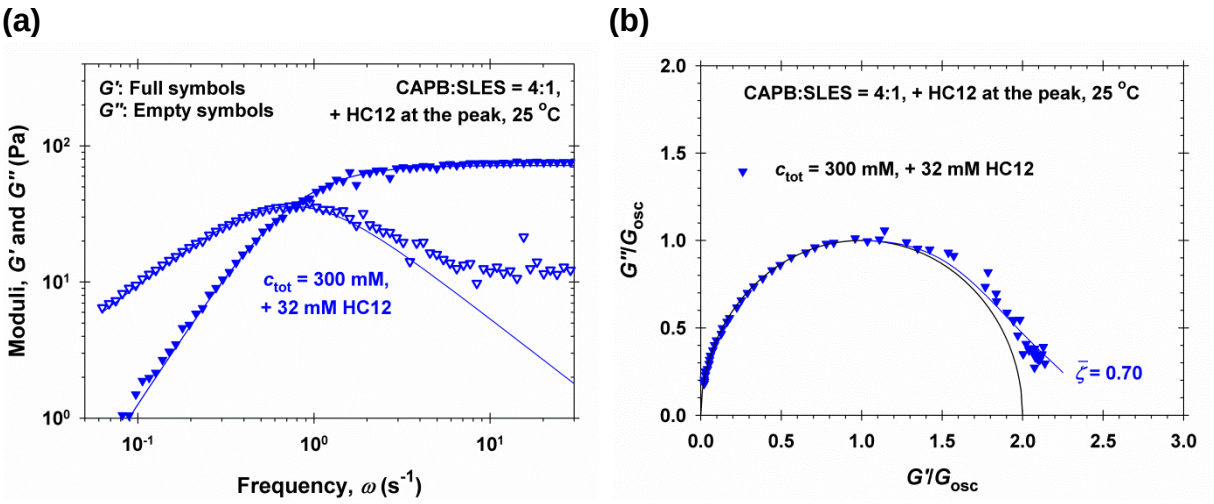

Figure S5. Frequency sweep data for the ternary micellar solution, for which the HC12 concentration (32 mM HC12) corresponds to the viscosity peak position at total surfactant (CAPB + SLES) concentration c_{tot} = 300 mM. (a) The storage and loss moduli, G' and G'', are plotted versus the angular frequency ω. The solid lines are drawn in accordance with the pure Maxwell model. (b) The Cole-Cole plot depicts G''/G_{osc} vs G'/G_{osc}, where $G_{osc} = G_0/2$. The semicircle represents the pure Maxwellian behavior, whereas the solid line represents a fit of numerical data from Refs. 9 and 10.

A.5. NMR measurements, spectra, and interpretation

Diffusion-ordered NMR spectroscopy (DOSY) and ^{23}Na NMR spectroscopy were used for the investigation of the ternary micellar solutions containing CAPB, SLES and dodecanoic acid at 298 K. In these studies, the CAPB-to-SLES ratio was 7:3, which differs from CAPB/SLES = 4:1 in the remaining text.

A.5.1. ^{23}Na NMR – theoretical background

A nucleus with a spin quantum number I >1 possesses a nuclear quadrupole moment that couples with the electric field gradient at the nuclear site. If the quadrupolar nucleus is in a molecule (or an aggregate) with a fixed or preferred orientation with respect to the magnetic field B_0, the degeneracy of the Zeeman transitions is lifted to give 2I lines.[11]

In an isotropic solution, the completely random (Brownian) motion averages out the effect of the quadrupolar interaction. In a liquid-crystalline phase (anisotropic media), the molecular motion, though still fast, is anisotropic, which results in a residual quadrupole splitting. Therefore, the splitting pattern can be used to distinguish between isotropic and anisotropic phases.

In the case of ^{23}Na, the spin quantum number I is equal to 3/2. This means that in anisotropic media the ^{23}Na signal splits into three peaks with relative areas 3:4:3.[11] In isotropic systems, the three transitions are degenerate and give a single peak with a chemical shift corresponding to the central line of the triplet.

A.5.2. NMR measurements

All NMR spectra were measured on a Bruker Avance II+ 600 NMR spectrometer operating at 600 MHz for ^{1}H. For the DOSY spectra, we used a 5 mm dual broadband direct detection probe with a *z*-gradient coil that delivers maximum strength of 63 G/cm (BBO-*z* probe). For the ^{23}Na (solid-state) NMR spectra, we used a 4 mm solid-state CP/MAS dual broadband direct detection probe.

Diffusion NMR spectroscopy (DOSY). The DOSY spectra were acquired with the double stimulated echo pulse sequence, so as to eliminate possible convection effects during the experiments. Monopolar smoothed square-shaped gradient pulses and three spoiling gradients for the elimination of unwanted coherences were used. All spectra were recorded with spectral width of 9600 Hz and 16 K time domain data points in t_2 dimension. To sample the diffusion dimension (t_1) and to ensure complete signal attenuation, the gradient strength G was varied in 32 steps in a linear ramp between 6 and 95% of the maximum gradient output of the gradient unit. Diffusion delay of 450 ms, gradient pulse length of 10 ms, 64 scans for each gradient strength increment and a relaxation delay of 3 s were selected. The spectra were processed with an exponential window function (line broadening factor of 2), 16 K data points in the chemical shift dimension and 1 K data points in the diffusion dimension, using the fitting routine integrated into the Topspin2.1 package. Both the inverse Laplace transform and the multi-exponential fitting with the Stejskal-Tanner equation, adapted for the particular pulse sequence, give comparable results within the limit of the experimental error.

Each of the obtained DOSY spectra represents a two dimensional (2D) matrix with the chemical shifts of the signals (in ppm) in the horizontal scale and the diffusion coefficients (in logarithmic units) in the vertical scale. At the top of the 2D spectrum, we have the ^{1}H NMR spectrum of the system. To the left of the 2D spectrum, we have the diffusion profile of the studied system, taken as a sum of the columns along the chemical shifts of the signals between 5 and 0 ppm. The peaks in the diffusion profile correspond to the diffusion coefficients of the respective surfactant molecules / aggregates.

^{23}Na NMR spectroscopy. To distinguish between isotropic and liquid-crystalline phases, we used the solid-state NMR equipment. We compared our micellar solutions to a test

sample with the following composition: 11.5 wt% SDS, 3 wt% CAPB and 3.5 wt% HC12 (lauric acid) in H_2O. The latter surfactant mixture has been studied by both ^{23}Na and diffusion NMR, proving that it represents a lyotropic discotic nematic phase N_D.[12]

Our micellar solutions and the test sample were probed by ^{23}Na solid-state NMR. During each measurement, the rotor with the sample was at 54.7° (a magic angle) with respect to the magnetic field B_0. The measurements were performed: (i) immediately after insertion of the rotor in the magnet; (ii) after 24 hours during which the rotor was kept parallel to the magnetic field B_0; and (iii) after 24 hours during which the rotor was kept perpendicular to the magnetic field B_0. The NMR spectra were measured with a spectral width of 375 ppm (59 kHz); 32 K data points in the time domain and 2048 accumulations.

A.5.3. Results and discussion

The results from the diffusion NMR measurements are summarized in Table S1. The calculated self-diffusion coefficients D_s are mean values determined from two experiments with different diffusion delays. From Table S1, for 70 mM CAPB (well-above the CMC), we see that the spherical micelles, $d_H \approx 5.6$ nm, are the dominant form of self-assembly. In the case of 30 mM SLES (well-above the CMC), the surfactant aggregates, $d_H \approx 5.4$ nm, are also spherical in shape. These micelle diameters are in excellent agreement with what is expected from molecular size considerations.

Table S1 also shows that the self-diffusion coefficient D_s for HC12 corresponds to free fatty acid monomers. Apart from these free monomers, the remaining dodecanoic acid forms crystallites that sediment during the measurement.

Next, we will discuss the DOSY results for the ternary micellar solutions, which contain CAPB, SLES and HC12. As shown in Table S1, the effective (micelle) diameters d_H are larger than 150 nm, meaning that the mixed surfactant aggregates are non-spherical. Assuming that the micelles are rodlike with a rod diameter d = 5.6 nm, we can calculate the rod length L using:[13]

$$d_H = \frac{L}{\ln(L/d)}, \qquad L >> d \text{ (thin rod)} \tag{A.10}$$

Using eq A.10, for d_H = 150 nm and d = 5.6 nm, we have L = 730 nm. Again, using eq A.10, for d_H = 200 nm and d = 5.6 nm, we have L = 1050 nm. These results indicate that long rod-like (even wormlike) micelles may form in the ternary mixtures due to synergistic micellar growth. The latter is mainly induced by the addition of HC12, which serves as a nonionic

spacer between the negatively-charged (SLES) headgroups, thus suppressing the intramicellar electrostatic repulsion.

Table S1. Self-diffusion Coefficients D_s and Effective Hydrodynamic Diameters d_H of the Micelles Formed in Solutions Containing CAPB, SLES, and HC12. Here, η_w = 1.09 mPa·s Is the Viscosity of the Solvent (Deuterium Oxide; D_2O).[5]

Surfactants	**Fatty acid**	D_s **(μm²/s)**	$d_H = \frac{kT}{3\pi\eta_w D_s}$ **(nm)**
70 mM CAPB	-	71	5.6
30 mM SLES	-	74	5.4
-	18 mM HC12	570	0.70*
70 mM CAPB + 30 mM SLES	14 mM HC12	2.0	200
	18 mM HC12	2.7	150

* Corresponds to free fatty acid molecules

To discriminate between isotropic and liquid-crystalline samples, we employed ^{23}Na NMR spectroscopy. First, we analyzed the test sample that contains 11.5 wt% SDS, 3 wt% CAPB and 3.5 wt% HC12 (lauric acid) in H_2O. Figure S6 shows that all ^{23}Na NMR spectra possess a characteristic quadrupolar splitting with relative areas of the triplet components being 3:4:3. In Figure S6a, the spectrum, acquired immediately after insertion of the rotor in the magnet, shows a narrow central peak and two wide satellites, where the satellites full width at half maximum (FWHM) is 725 Hz. In Figure S6b, the spectrum was measured after 24 hours during which the rotor was kept in the magnet with an orientation parallel to the magnetic field B_0. As a result, the satellites FWHM was reduced to 233 Hz, which indicates further alignment of the micelles with respect to the magnetic field B_0. In Figure S6c, the spectrum was measured after 24 hours during which the rotor was kept perpendicular to the direction of the magnetic field B_0. In this case, the satellites FWHM slightly increases to 263 Hz compared to the previous case. These findings confirm the results obtained by Colafemmina et al.,[12] that is, the test sample represents a liquid-crystalline discotic phase.

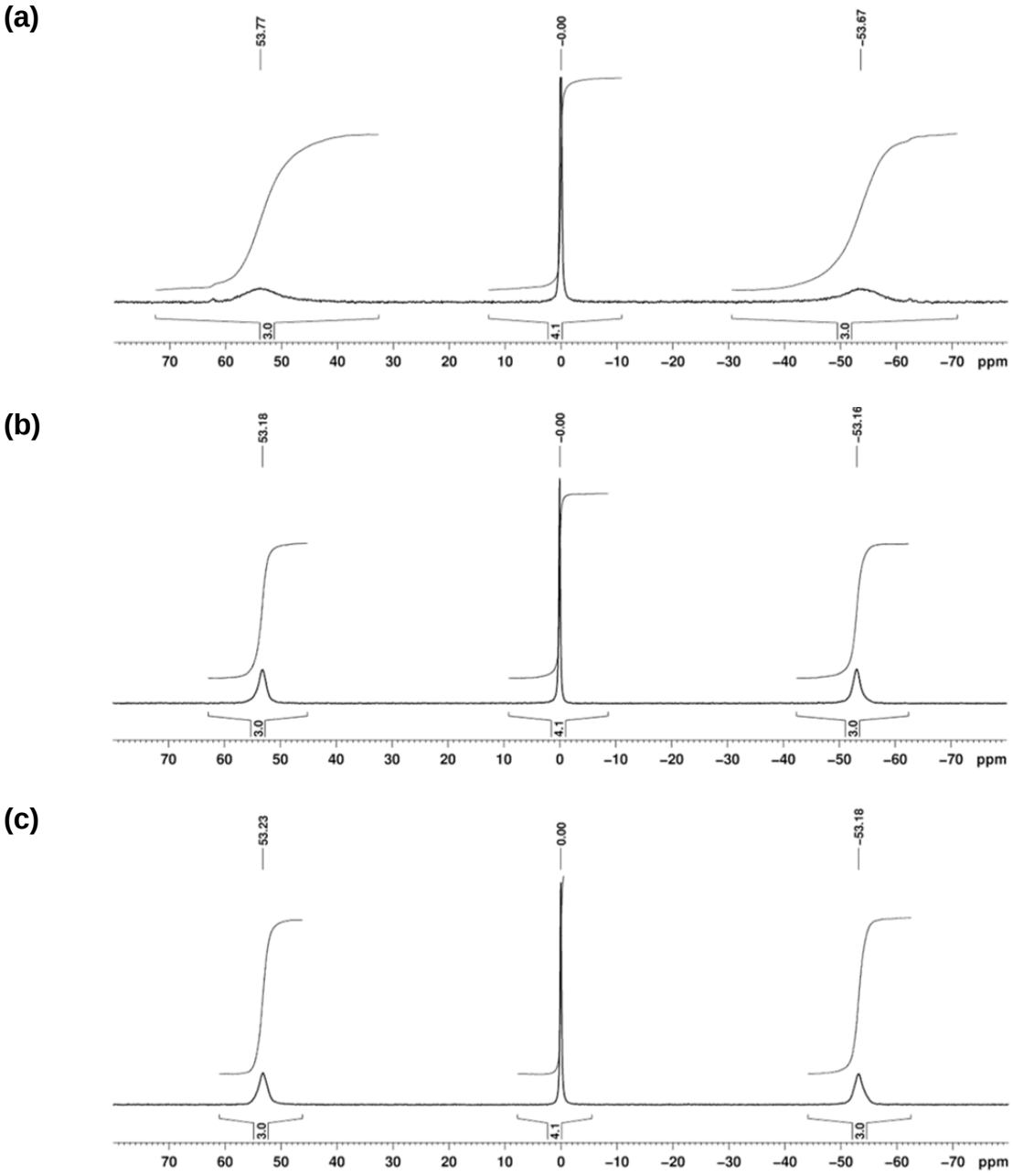

Figure S6. ^{23}Na NMR spectra of the test system (11.5 wt% SDS, 3 wt% CAPB and 3.5 wt% HC12 in H_2O) obtained at a magic angle and the following conditions: (a) immediately after insertion of the rotor in the magnet; (b) after 24 hours during which the rotor was kept parallel to the magnetic field B_0; (c) after 24 hours during which the rotor was kept perpendicular to the magnetic field B_0.

In contrast to the spectra above, the ^{23}Na NMR spectra of our micellar solutions show only one signal regardless of the rotor orientation and the time spent in the magnet. The absence of quadrupole splitting reflects the lack of ^{23}Na orientation effects. Such effects are to be expected in the case of anisotropic (liquid-crystalline) media. These results demonstrate

that our samples represent isotropic micellar solutions consisting of discrete aggregates rather than liquid-crystalline phases aligned in the magnetic field.

A.6. Polarized-light microscopy

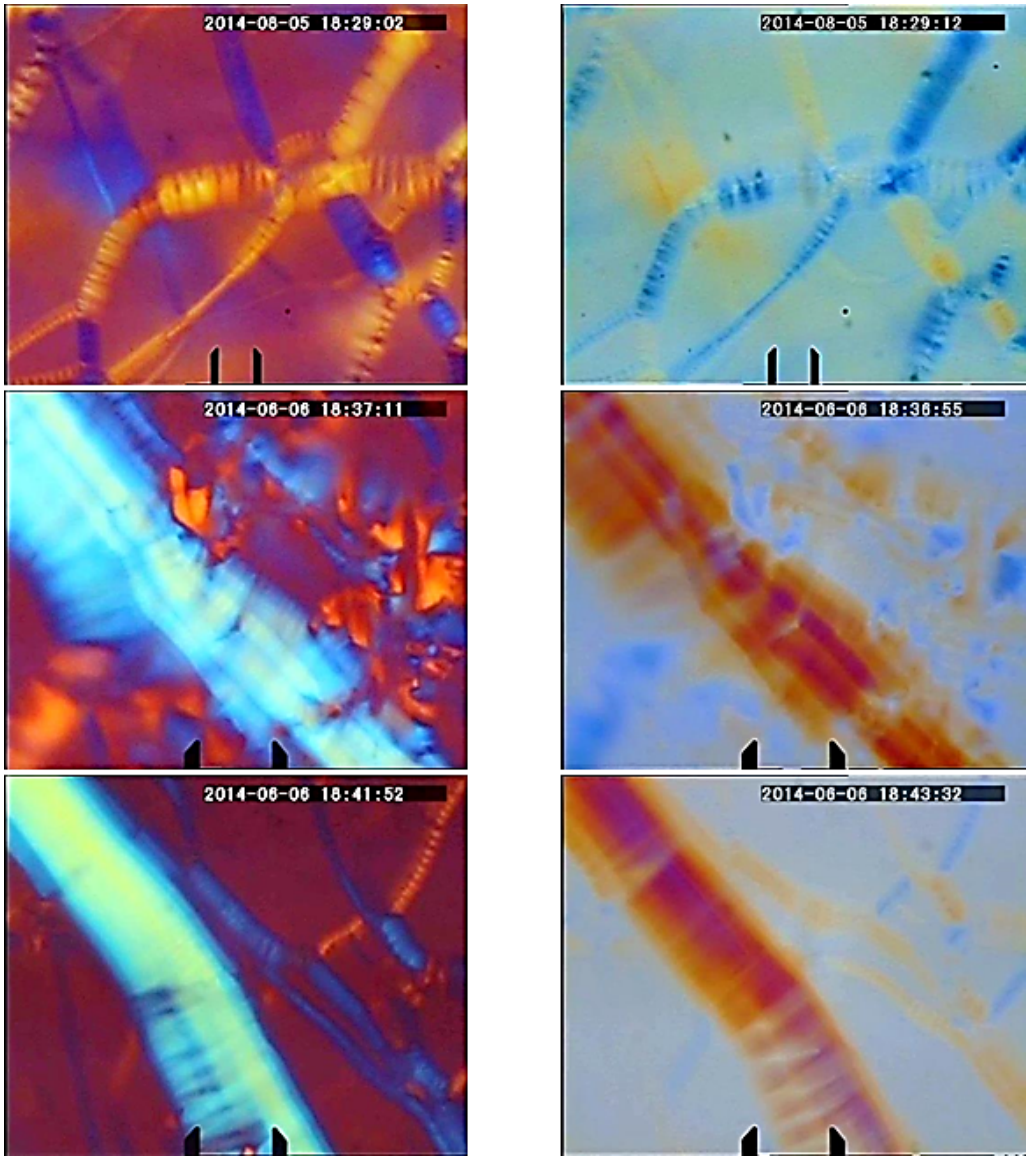

Figure S7. In the test sample, patterns (textures) that are typical for liquid-crystalline phases are observed by polarized-light microscopy. In the left column, the angle between the polarizer and the analyzer is 0°. In the right column, the angle is 90°.

References

(1) *Product specification sheet of TEGO® Betain F50*, Evonik Nutrition & Care GmbH, Evonik Industries AG, Germany.

(2) *Supporting information* from Georgieva, G. S.; Anachkov, S. E.; Lieberwirth, I.; Koynov, K.; Kralchevsky, P. A. Synergistic Growth of Giant Wormlike Micelles in Ternary Mixed Surfactant Solutions: Effect of Octanoic Acid. *Langmuir* **2016**, *32*, 12885–12893.

(3) Harned, H. S.; Owen, B. B. *The Physical Chemistry of Electrolytic Solutions*; 2nd ed., Reinhold Publishing Corp.: New York, 1950.

(4) Ravdel, A. A.; Ponomareva, A. M. (Eds.), *Concise Handbook of Physicochemical Quantities*; 8th ed., Khimiya: Leningrad, 1983 [in Russian].

(5) Haynes, W. M. (Ed.), *CRC Handbook of Chemistry and Physics*; 95th ed., CRC Press: Boca Raton, 2014 – 2015.

(6) Weers, J. G.; Rathman, J. F.; Axe, F. U.; Crichlow, C. A.; Foland, L. D.; Scheuing, D. R.; Wiersema, R. J.; Zielske, A. G. Effect of the Intramolecular Charge Separation Distance on the Solution Properties of Betaines and Sulfobetaines. *Langmuir* **1991**, *7*, 854–867.

(7) Tzocheva, S. S.; Kralchevsky, P. A.; Danov, K. D.; Georgieva, G. S.; Post, A. J.; Ananthapadmanabhan, K. P. Solubility limits and phase diagrams for fatty acids in anionic (SLES) and zwitterionic (CAPB) micellar surfactant solutions. *J. Colloid Interface Sci.* **2012**, *369*, 274–286.

(8) Lucassen, J. Hydrolysis and Precipitates in Carboxylate Soap Solutions. *J. Phys. Chem.* **1966**, *70*, 1824–1830.

(9) Turner, M. S.; Cates, M. E. Linear viscoelasticity of living polymers: A quantitative probe of chemical relaxation times. *Langmuir* **1991**, *7*, 1590−1594.

(10) Kern, F.; Lemarechal, P.; Candau, S. J.; Cates, M. E. Rheological properties of semidilute and concentrated solutions of cetyltrimethylammonium bromide in the presence of potassium bromide. *Langmuir* **1992**, *8*, 437−440.

(11) Laszlo, P. Sodium-23 Nuclear Magnetic Resonance Spectroscopy. *Angew. Chemie Int. Ed. English* **1978**, *17*, 254–266.

(12) Colafemmina, G.; Recchia, R.; Ferrante, A. S.; Amin, S.; Palazzo, G. Lauric Acid-Induced Formation of a Lyotropic Nematic Phase of Disk-Shaped Micelles. *J. Phys. Chem. B* **2010**, *114*, 7250–7260.

(13) Kralchevsky, P.; Danov, K.; Denkov, N. Chemical Physics of Colloid Systems and Interfaces. In *Handbook of Surface and Colloid Chemistry, Third Edition*; CRC Press, 2008; pp 197–377.